23 High Redshift Supernovae from the IfA Deep Survey[1,2]: Doubling the SN Sample at $z > 0.7$

Brian J. Barris[3], John L. Tonry[3], Stéphane Blondin[4], Peter Challis[5], Ryan Chornock[6], Alejandro Clocchiatti[7], Alexei V. Filippenko[6], Peter Garnavich[8], Stephen T. Holland[9], Saurabh Jha[6], Robert P. Kirshner[5], Kevin Krisciunas[10,11], Bruno Leibundgut[4], Weidong Li[6], Thomas Matheson[5], Gajus Miknaitis[12], Adam G. Riess[13], Brian P. Schmidt[14], R. Chris Smith[10,11], Jesper Sollerman[15], Jason Spyromilio[4], Christopher W. Stubbs[12], Nicholas B. Suntzeff[10,11], Hervé Aussel[3], K. C. Chambers[3], M. S. Connelley[3], D. Donovan[3], J. Patrick Henry[3], Nick Kaiser[3], Michael C. Liu[3,16], Eduardo L. Martín[3], and Richard J. Wainscoat[3]

ABSTRACT

We present photometric and spectroscopic observations of 23 high redshift supernovae spanning a range of $z = 0.34 - 1.03$, 9 of which are unambiguously classified as Type Ia. These supernovae were discovered during the IfA Deep Survey, which began in September 2001 and observed a total of 2.5 square degrees to a depth of approximately $m \approx 25 - 26$ in RIZ over 9-17 visits, typically every 1-3 weeks for nearly 5 months, with additional observations continuing until April 2002. We give a brief description of the survey motivations, observational strategy, and reduction process. This sample of 23 high-redshift supernovae includes 15 at $z \geq 0.7$, doubling the published number of objects at these redshifts, and indicates that the evidence for acceleration of the universe is not due to a systematic effect proportional to redshift. In combination with the recent compilation of Tonry et al. (2003), we calculate cosmological parameter density contours which are consistent with the flat universe indicated by the CMB (Spergel et al. 2003). Adopting the constraint that $\Omega_{total} = 1.0$, we obtain best-fit values of $(\Omega_m,\Omega_\Lambda)=(0.33, 0.67)$ using 22 SNe from this survey augmented by the literature compilation. We show that using the empty-beam model for gravitational lensing does not eliminate the need for $\Omega_\Lambda > 0$. Experience from this survey indicates great potential for similar large-scale surveys while also revealing the limitations of performing surveys for $z > 1$ SNe from the ground.

Subject headings: cosmological parameters – distance scale – galaxies: distances and redshifts – supernovae: general

[1]CFHT: Based in part on observations obtained at the Canada-France-Hawaii Telescope (CFHT) which is operated by the National Research Council of Canada, the Institut National des Science de l'Univers of the Centre National de la Recherche Scientifique of France, and the University of Hawaii. CTIO: Based in part on observations taken at the Cerro-Tololo Inter-American Observatory. Keck: Some of the data presented herein were obtained at the W.M. Keck Observatory, which is operated as a scientific partnership among the California Institute of Technology, the University of California, and the National Aeronautics and Space Administration. The Observatory was made possible by the generous financial support of the W.M. Keck Foundation. Magellan: Based in part on observations from the 6.5 m Baade telescope operated by the Observatories of the Carnegie Institution of Washington for the Magellan Consortium, a collaboration between the Carnegie Observatories, the University of Arizona, Harvard University, the University of Michigan, and the Massachusetts Institute of Technology. UH: Based in part on observations with the University of Hawaii 2.2-m telescope at Mauna Kea Observatory, Institute for Astronomy, University of Hawaii. VLT: Based in part on observations obtained at the European Southern Observatory, Paranal, Chile, under programs ESO 68.A-0427.

[2]Based in part on observations with the NASA/ESA *Hubble Space Telescope*, obtained at the Space Telescope Science Institute, which is operated by the Association of

1. Introduction

1.1. Searching for Cosmological SNe Ia– Past and Future

It has now been over five years since the announcements by the High-z Supernova Search Team (Riess et al. 1998) and Supernova Cosmology Project (Perlmutter et al. 1999) of evidence for the acceleration of the expansion of the universe and the inferred presence of a non-zero cosmological constant. Since the implications of this result are so profound for cosmology and our understanding of fundamental physics, it has been the subject of intense scrutiny from several different directions with attempts to test for further confirmation or any sign of problems.

One goal of the immediate follow-up work was obtaining better measurements of low and moderately-high redshift ($z < 0.5$) Type Ia supernovae (SNe Ia) to increase the confidence in their use as standard candles for cosmological purposes. Near-IR observations (Riess et al. 2000) showed no evidence for extragalactic dust in a single SN Ia at $z \approx 0.5$, and spectra of a separate object at a similar redshift (Coil et al. 2000) compared very closely with nearby SNe Ia, showing no sign of spectroscopic evolution. Sullivan et al. (2003) demonstrated that host galaxy extinction is unlikely to cause the observed dimming of high-redshift SNe, by comparing Hubble diagrams as a function of galaxy morphology (see also Williams et al. (2003) for a discussion of host galaxy-SNe correlations). However, Leibundgut (2001) presented evidence that distant SNe Ia are significantly bluer than the nearby sample, possibly indicating photometric evolution that could bedevil analyses which assume that color corrections can be made based on comparison to local SNe Ia.

There have also been continued attempts to discover supernovae at even higher redshifts. An extreme case is the serendipitous reimaging in the Hubble Deep Field of SN 1997ff (Riess et al. 2001), which added intriguing additional evidence for an earlier period of deceleration, with the caveats that it is only a single object and potentially gravitational lensed (Benitéz et al. 2002). The sample size of high-z objects has been substantially added to by recent campaigns described by Tonry et al. 2003 (8 SNe Ia between $0.3 < z < 1.2$), as well as Knop et al. 2003 (11 SNe Ia between $0.36 < z < 0.86$).

The ability to discover large numbers of high-redshift supernovae with reliability was made possible by the development of wide-field cameras with large-format CCDs on large telescopes. Observing time on these instruments is extremely precious, and standard practice is to obtain time for a template observation, followed some weeks later by a second epoch from which to subtract

Universities for Research in Astronomy (AURA), Inc., under NASA contract NAS 5-26555. This research is primarily associated with proposal GO-09118.

[3]Institute for Astronomy (IfA), University of Hawaii, 2680 Woodlawn Drive, Honolulu, HI 96822; barris@ifa.hawaii.edu, jt@ifa.hawaii.edu, aussel@ifa.hawaii.edu, chambers@ifa.hawaii.edu, msc@galileo.ifa.hawaii.edu, donovan@ifa.hawaii.edu, henry@ifa.hawaii.edu, kaiser@ifa.hawaii.edu, liu@ifa.hawaii.edu, ege@ifa.hawaii.edu, rjw@ifa.hawaii.edu

[4]European Southern Observatory, Karl-Schwarzschild-Strasse 2, Garching, D-85748, Germany; sblondin@eso.org, bleibund@eso.org, jspyromi@eso.org

[5]Harvard-Smithsonian Center for Astrophysics, 60 Garden Street, Cambridge, MA 02138; pchallis@cfa.harvard.edu, kirshner@cfa.harvard.edu, tmatheson@cfa.harvard.edu

[6]University of California, Department of Astronomy, 601 Campbell Hall, Berkeley, CA 94720-3411; rchornock@astro.berkeley.edu, alex@astro.berkeley.edu, sjha@astro.berkeley.edu, weidong@astro.berkeley.edu

[7]Pontificia Universidad Católica de Chile, Departmento de Astronomía y Astrofísica, Casilla 306, Santiago 22, Chile; aclocchi@astro.puc.cl.

[8]University of Notre Dame, Department of Physics, 225 Nieuwland Science Hall, Notre Dame, IN 46556-5670; pgarnavi@miranda.phys.nd.edu

[9]Code 662.20, Goddard Space Flight Centre, Greenbelt, MD 20771-0003; sholland@milkyway.gsfc.nasa.gov

[10]Cerro Tololo Inter-American Observatory, Casilla 603, La Serena, Chile; kkrisciunas@noao.edu, csmith@ctio.noao.edu, nsuntzeff@noao.edu

[11]Las Campanas Observatory, Casilla 601, La Serena, Chile

[12]University of Washington, Department of Astronomy, Box 351580, Seattle, WA 98195-1580; gm@u.washington.edu, stubbs@astro.washington.edu

[13]Space Telescope Science Institute, 3700 San Martin Drive, Baltimore, MD 21218; ariess@stsci.edu

[14]The Research School of Astronomy and Astrophysics, The Australian National University, Mount Stromlo and Siding Spring Observatories, via Cotter Rd, Weston Creek PO 2611, Australia; brian@mso.anu.edu.au

[15]Stockholm Observatory, AlbaNova, SE-106 91 Stockholm, Sweden; jesper@astro.su.se

[15]Hubble Fellow

the first epoch and thus detect supernovae (see Schmidt et al. 1998). The observations necessary to obtain a complete photometric light curve of confirmed SNe Ia are then made with other telescopes that can target individual objects, and on which access to time is somewhat less competitive. Spectroscopic confirmation that a candidate is indeed a SN Ia requires significant time on 8–10-m class telescopes, and the amount of such time that can be obtained is often the limiting factor for supernova surveys.

The coming years will see a tremendous increase in the number of astronomical surveys taking advantage of the ability of these wide-field imaging cameras to cover large regions of sky. In a new twist, these surveys will observe large areas repeatedly in order to explore the astronomical time domain in unprecedented ways. This will allow better understanding of a wide range of transient objects such as asteroids, microlensing events, active galactic nuclei (AGN), and supernovae, as well as potentially unveiling previously unknown time variable phenomena.

This trend has already begun to a limited extent with such projects as the Deep Lens Survey (Wittman et al. 2002) and Sloan Digital Sky Survey (York et al. 2000), which in late 2002 began repeat coverage of certain fields in order to search for variable objects (Miknaitis et al. 2002). Among other surveys underway is ESSENCE (http://www.ctio.noao.edu/wproject, Smith et al. 2002), a five-year program to discover hundreds of SNe Ia over a wide redshift range ($0.2 < z < 0.7$) in order to measure the cosmological equation of state. The exploration of the wide-field, temporal-variability domain is scheduled to culminate with truly massive undertakings such as the CFH Legacy Survey (http://www.cfht.hawaii.edu/Science/CFHLS) and PanSTARRS (http://poi.ifa.hawaii.edu, Kaiser et al. 2002).

The *Hubble Space Telescope* (*HST*) has also recently entered the fray with the Advanced Camera for Surveys (ACS; Ford et al. 1998), giving it wide-field capability. Several objects have been discovered through observations of the Hubble Deep Field North (Blakeslee et al. 2002), and in late 2002 a campaign was begun to discover supernovae out to the redshift $z \approx 1.7$ through strategic placement of GOODS survey observations (Riess 2002), already yielding numerous objects (Riess et al. 2003). Finally, the extreme of aspirations is the proposed Supernova Acceleration Probe (SNAP) (Nugent 2001), a satellite mission specifically designed to discover and monitor huge numbers of SNe Ia out to $z \approx 1.7$.

1.2. The IfA Deep Survey

Beginning in September 2001, a collaboration of astronomers from the Institute for Astronomy (IfA) at the University of Hawaii-Manoa undertook the IfA Deep Survey, using wide-field imagers atop Mauna Kea, Hawaii. This project imaged 2.5 square degrees in multiple colors (RIZ) roughly every 2–3 weeks for approximately 5 months, with observations continuing until April 2002. The major motivation for separating the individual nights in this manner was to discover and follow large numbers high-redshift supernovae. The survey was designed to accommodate investigations of a wide range of scientific goals, including searches for substellar objects, galactic structure studies, variable object searches (particularly supernovae), and galaxy clustering studies. Preliminary analysis of survey data has already yielded at least one substellar object (Liu et al. 2002), and scores of both high redshift supernova (Barris et al. 2001, 2002) and brown dwarf candidates (Graham 2002; Martín et al., in preparation).

The novel feature of this campaign was the use of survey observations to follow SNe Ia as well as find them. No prior supernova campaign has been performed in this manner. At the beginning of any survey, many supernovae will be discovered well past maximum light, which will not be suitable for cosmological studies. Similarly, supernovae which are discovered before or at maximum light at the end of the survey will not have sufficient follow-up observations to be useful. However, all of the supernovae discovered in the middle of a continuous survey will have observations on the rising portion of the light curve as well as far into the decline, giving sufficient coverage for light curve fitting and hence distance determination.

In this paper we describe the IfA Deep Survey and data reduction as well as results from the supernova search. In Section 2 we describe the survey observations. In Section 3 we give a brief description of the pipeline data reduction process, which produces the final images to be used by all

the collaborators. Section 4 describes the supernova search. Sections 5 and 6 discuss the distance measurements and cosmological analysis, and Section 7 gives our conclusions.

2. Observations

2.1. Survey Science Observations

For most of the scientific goals of the IfA Deep Survey, the primary concern was overall survey depth. The most important factors for the supernova search component were sufficient depth on individual nights to detect high-redshift supernovae and separation of the nights so as to allow for continual detection and follow-up throughout the duration of the survey. The primary instruments used were Suprime-Cam (Miyazaki et al. 1998) on the Subaru 8.2-m telescope, and the 12K camera (Cuillandre et al. 1999) on the Canada-France-Hawaii 3.6-m telescope (CFHT).

The survey strategy was designed to provide for the discovery and follow-up of 10–25 SNe Ia with $0.9 < z < 1.2$ in order to distinguish whether the evidence from SNe Ia at lower redshift for an accelerating universe could actually be due to a systematic effect proportional to redshift rather than an indication of a non-zero cosmological constant. The rates of high-redshift supernovae are still quite uncertain (see Pain et al. 1996, 2002 and Tonry et al. 2003), but the rate of SNe Ia in our desired redshift range is approximately 2–5 per sq. deg. per month, depending on when the individual images are taken. The peak brightness of a SN Ia at $z = 1.2$ is about $I = 24.3$ and $Z = 23.6$, so each survey night was designed to provide a signal-to-noise ratio (S/N) of 11 in I band and S/N = 7 in Z band at these magnitudes, assuming $0.75''$ seeing. This is a bit less S/N than ideal for Z band, but some observations were taken with much better seeing which went deeper (and conversely, some were taken with worse seeing and therefore went shallower). In addition, the R band images, designed for S/N = 10 per observation, can be used to help distinguish SNe Ia from SNe II, based on the redder color of high-redshift SNe Ia (see Section 4.3 below).

Fields and observational cadence were chosen to meet the necessary requirements of all the scientific programs. Primary considerations included a spread in right ascension to allow for continuous observation throughout a single night over several fall and winter months from Mauna Kea; low galactic extinction; and whether previous observations, in the same or other wavelength regions, could be used to augment the scientific objectives. Five 0.5-square degree fields were chosen for the survey. Central coordinates of the selected fields are given in Table 1. The field at 02^h27^m (Field 0230) was previously used for high-redshift surveys by the High-z Supernova Search Team (see Tonry et al. 2003). Field 0848 was chosen to overlap with previous radio observations, and Field 1052 ("Lockman Hole," see Lockman, Jahoda, & McCammon 1986) was chosen for a wide range of prior multi-wavelength studies (x-ray: Hasinger et al. 1993; radio: de Ruiter et al. 1997, and Ciliegi et al. 2003; IR: Taniguchi, Kawara, & Matsuhara 1999, and Fadda et al. 2002).

The 12K camera consists of twelve 2048x4096 pixel CCDs, with a field of view of $45'$ x $30'$ (0.375 sq. degrees) and a pixel scale of $0.206''$/pixel. Survey fields were observed with a Mould I filter, with a central wavelength of 8223 Å and a width of 2164 Å.

The Suprime-Cam instrument, consisting of a mosaic of ten 2048x4096 pixel CCDs, covers a $34'$ x $27'$ field of view (0.255 sq. degrees), and has an image scale of $0.20''$/pixel. The survey fields were observed with Suprime-Cam with Cousins R and I and Subaru Z filters. The Z filter at Subaru has an effective wavelength of 9195 Å and FWHM of 1410 Å (Fukugita et al. 1996). Each of the five fields was covered by two overlapping Suprime-Cam fields-of-view (FOVs). The central coordinates for the pair of Suprime-Cam pointings for each field are given in Table 1. For four of the fields (all except for Field 1052), the two Suprime-Cam fields-of-view were rotated by 90 degrees relative to the 12K FOV. Thus the coverage with two Suprime-Cam fields-of-view was approximately $34'$ x $54'$ (≈0.5 square degrees), compared to $30'$ x $45'$ (accounting for the orientation) with the 12K. For field 1052 the appropriate comparison is $34'$ x $54'$ with Suprime-Cam and $45'$ x $30'$ with 12K, so that in this configuration there were regions on the edge of the field which were imaged with the 12K but not with Suprime-Cam, and vice versa, while for the other fields the 12K FOV is completely covered by the Suprime-Cam footprint (see Figure 1 for an illustration).

The bulk of the survey took place over 8 full nights and 5 half nights with Suprime-Cam on Subaru from October 2001 through April 2002. Target fields were also observed between 1 and 5 times with queue-scheduled observations with the 12K at CFHT. Not all nights were photometric, and exposure times occasionally varied depending on conditions. A summary of observations, including date, exposure time, and mean seeing value, is given in Tables 2 (CFHT 12K) and 3 (Suprime-Cam).

Exposure times were chosen to achieve approximately the same survey depth in the three filters, though the required exposure times for Z were impractically long, and so this filter did not go as deep as R and I. The long readout time for Suprime-Cam was also a major factor. For a typical night, 5-σ point source sensitivities were roughly 25.8 in R, 25.2 in I, and 24.2 in Z. When the entire survey is combined, the 5-σ point source depth of the summed images is approximately 27.3 in R, 26.7 in I, and 25.6 in Z, varying from field to field due to differences in integration time as well as seeing conditions on nights when a particular field might be more heavily represented. See Figure 2 for a comparison of the depth and area coverage of the IfA Deep Survey with several other recent surveys, illustrating where this survey lies in area vs. sensitivity parameter space.

2.2. Astrometric Observations

In addition to the survey science observations, we also obtained shorter exposures in order to construct astrometric catalogs of the target fields. These observations, taken with the CFHT 12K camera, were 120 s in all bands (Mould R, Mould I, Z). One advantage of these shorter images is that they create a photometric overlap with an external reference, the USNO-A catalog (Monet 1998), since the much deeper science images discussed in the previous section do not contain any non-saturated stars from this catalog. The images of each field were taken with half-CCD offsets to determine astrometry over the entire survey area.

Object detection software was run on the astrometric images (findpeaks from the imcat package, see http://www.ifa.hawaii.edu/∼kaiser) to construct a catalog of objects to register with the USNO-A catalog. Solutions for image mapping parameters were then obtained using a process developed for weak lensing studies (see Kaiser (2000) for a detailed mathematical description of the method, and Kaiser et al. (1999) for a more practical summary). Stars brighter than $m \approx 21$ are identified in the astrometric images as well as the USNO-A catalog, and a large matrix equation mapping CCD coordinates to sky tangent plane coordinates is fit by a cubic polynomial. We then iterate until the process converges, rejecting outlying points after each step. Great care was needed so as not to mistakenly reject large groups of stars in a given region which may show a systematic offset due to a single problematic star.

After achieving an acceptable solution (typically requiring 4–6 iterations), more sensitive object detection was run on the astrometric images to augment the catalog with stars faint enough to overlap with the much deeper science images. Going deeper means that many objects in the reference catalog will be faint galaxies rather than stars, but since they are stellar in appearance they are still suitable for astrometry.

The end product of this process was a catalog of stars with extremely accurate relative astrometry (to a fraction of a pixel, i.e. better than 0.1 arcseconds), extending to very faint magnitudes ($m \approx 22$ for R, I and $m \approx 21$ for Z). The catalogs range in size from about 4000 stars for Fields 0230, 0848, and 1052; to 7000 for Field 0438; to more than 9500 for Field 0749, which is at a lower galactic latitude than the other fields.

2.3. Photometric Observations

Photometric observations were obtained at the CTIO 1.5-m and UH 2.2-m telescopes. Landolt standards (Landolt 1992) and spectrophotometric standards, which have Landolt magnitudes as well as synthetic Z magnitudes, were observed in $BVRIZ$ (Johnson BV, Cousins RI, and Z as described in Tonry et al. 2003) to set the magnitude scale of the survey target fields.

Flux measurements for the standard stars were calculated using $14''$ diameter aperture magnitudes of isolated local standards in each field. For each night and filter an atmospheric extinction coefficient and a color term was calculated. This fit to airmass and color typically showed a scatter of 0.02 mags, due to the usual difficulties of data reduction: sky errors, flatfielding imperfec-

tions, atmospheric transparency variations, CCD non-linearity, shutter timing errors, and variations due to PSF or scattered light.

Our Z band observations were calibrated by observing a series of Landolt stars, whose magnitudes were derived by integrating their spectrophotometry (Suntzeff, in preparation) with our bandpass defined by the CTIO natural system. This system is defined to have $(V - Z) = 0$ for Vega.

The astrometric catalogs described above have accurate relative photometry, and the CTIO 1.5-m and UH 2.2-m observations allowed us to put them on an accurate absolute scale. Calibration of the 0230 field was described by Tonry et al. (2003), wherein cross-checks with the Sloan Digital Sky Survey (SDSS, Stoughton et al. 2002) indicate an accuracy as good as the SDSS zero-point uncertainty of 0.04 magnitudes.

3. Pipeline Reductions

Survey science images were initially reduced using a reduction pipeline created specifically for this purpose at the IfA. The majority of the pipeline consisted of custom scripts using the Vista image display and manipulation software. The search for high-redshift supernovae was a time-critical mandate for the reductions, so the pipeline was designed to be as efficient as possible. Initial processing took place as soon as the data were received via FTP from the telescope. A second processing, free of time pressures and with slight modifications, was performed after the conclusion of the survey.

The images were first bias subtracted using a median value from pixels in the overscan region of each chip. For the Subaru data, a median superflat image was constructed from all the images for a given chip and filter from the entire night. Images were flattened by dividing by this superflat. For the CFHT 12K images, dome flats were used to flatten the data, and a fringe frame was constructed from the entire night. The images were flattened by the dome flat image, and the fringe frame subtracted. The Suprime-Cam observations had small enough fringing (less than a few percent) that division of the fringe light instead of subtraction did not significantly affect photometry. Bad pixels and other chip defects were removed using a mask created at the start of the campaign, which proved to be sufficient for the entire survey. Any remaining tilt in the sky was subtracted, and the sky normalized to a value of 1000 for ease of software compatibility.

The flattened images were then mapped to the astrometric catalogs of the survey fields through detecting (via SExtractor) and matching stars (using a similar process as described for the astrometric observations, though now the custom-made astrometric catalogs were the reference, rather than the USNO-A catalog). Using these astrometric solutions, the images were warped onto a predefined coordinate system on a sky tangent plane. The final post-warp images used a pixel scale of $0.20''$/pixel, which is similar to both Suprime-Cam and CFHT 12K. The warping process conserves flux and uses a Jacobian to restore photometric accuracy lost by flatfielding. Since dividing by the flatfield in the pre-warp stage equalizes surface brightness regardless of geometrical distortion of pixel area, and our warping conserves flux rather than surface brightness, the Jacobian is necessary for accurate photometry.

At this point cosmic ray (CR) rejection was done and the images combined. Performing CR rejection at this stage has the drawback of decreased sensitivity due to smearing of the cosmic rays during the warping, and thus many were not removed. For the goal of discovering supernovae, this was not an insurmountable problem, as individual dithers contributing to the final image of a candidate could be inspected. In the second processing, performed after the conclusion of the survey, the cosmic ray rejection was performed before, rather than after, the warping stage. Images were registered by adaptively finding subimages for which integer pixel shifts gave sufficiently close registration, and cosmic ray rejection performed after the processing steps of flattening, pixel masking, etc. This resulted in a significant improvement in the removal of cosmic rays. After the CR rejection, the warping was performed with cosmic ray masked pixels treated the same as other bad pixels.

4. Supernova Search

4.1. Supernova Discovery

In order to perform the supernova search, previous I observations were subtracted from each new set of images to detect photometrically variable objects. Because our first set of observations, in September 2001, were taken with the CFHT 12K, subtractions from our first Subaru+SuprimeCam nights in October could only be done over the area in common with both telescope fields-of-view (the central 0.375 square-degrees of the 0.51 square-degrees covered by SuprimeCam). In subsequent months we possessed a complete set of templates which allowed for searching of the entire survey area.

Subtractions were performed largely in the same manner as for previous supernova searches (see Schmidt et al. 1998, Tonry et al. 2003). New software was written (Becker et al., in preparation), slightly modifying the algorithms of Alard (2000) and Alard & Lupton (1998) based on insights gleaned from searches for microlensing as well as past supernova campaigns. Pairs of observations to be subtracted were compared to determine the worse seeing night, with the better night then convolved to match PSFs. Flux levels were matched, and the images subtracted.

Two independent automatic search algorithms were run on the subtracted images to detect variable sources. The images were divided into regions 7 arcminutes on a side for ease of searching, and in a typical such region several dozen variable sources were detected. Approximately half of these were false positives such as diffraction spikes around saturated stars, or filter mismatches between CFHT and Subaru. A large number were variable stars and AGN, which are typically distinguished from supernovae by being a small fluctuation centered on a constant point source. All subtractions were searched visually by at least one person, aided by the automatic algorithms. In addition to the many false positives, the automatic detection programs missed some faint supernovae, but in general seemed to do a respectable job in finding objects when compared to well trained searchers. After the initial search was completed, candidate supernovae were inspected by an additional observer. The constituent images (typically a single I band observation was comprised of 3 separate dither positions) were also examined to weed out cosmic rays and moving objects.

Ideally, the fact that we had observations in three filters would have been extremely useful in distinguishing between SNe Ia and SNe II based on the difference in color at early times (at high redshifts, SNe II are much bluer than SNe Ia in RIZ). In practice, however, reducing and searching the I-band data alone consumed all available resources. Upon further inspection of the IfA Deep Survey observations we should be able to provide an excellent assessment of whether theoretical photometric discriminatory tests (see Poznanski et al. 2003) are actually useful for real-world surveys. We have already begun to use them for the purposes of augmenting our sample, as described in Section 4.3 below.

Our continuous search strategy did enable us to attempt to differentiate between the types of supernovae based on the shape of their early light curve. Type II SNe have extremely heterogeneous light curves (see Leibundgut & Suntzeff 2003, and references therein). One major subclass, the SNe II-P, exhibit a very short rise to maximum light, followed by a plateau in brightness. After a detection we were usually able to compare with an observation made a week or two previously. Quite often the supernova was present in this prior epoch but faint enough that it was not detected by our searchers, indicating a gradual rise, and hence a likely SN Ia rather than a SN II. Alternatively, if the object was not present at all in this previous epoch, it was more probably a SN II or a SN Ia at a much lower redshift.

After this rigorous inspection process candidates were prioritized and forwarded to the spectroscopic observers, who were usually already waiting at the telescope.

4.2. Spectroscopic Observations

Though the continuous nature of the IfA Deep Survey naturally provided for photometric follow-up of supernova candidates, guaranteeing successful spectroscopic follow-up was still problematic. The only possibility for supernova surveys is to rely on time allocation committees to schedule observing nights a few days after the photometric search observations and hope that supernova candidates for spectroscopy will be ready in time.

Complications can arise from many uncontrollable issues—the photometry night may have poor conditions, the searchers may encounter hardware and/or software problems, the timing between photometric and spectroscopic nights may end up being too short, among other pitfalls. Despite the difficulty involved, measurement of redshift and identification as a SN Ia is necessary to be able to use a supernova for cosmological purposes.

We arranged spectroscopic resources on many telescopes over the course of the IfA Deep Survey—primarily the Keck I and II telescopes, with the VLT also playing a major role, though it was unable to reach our northernmost fields. Additional spectroscopic observations were made with the Magellan telescope, though it was not used for identification of any of the high-z SNe Ia discussed here.

We observed a total of 63 objects spectroscopically during 6 separate observing runs (4 with Keck, in addition to one each with the VLT and Magellan) spaced throughout the duration of the survey. We were also able to observe a small number of supernova host galaxies in late 2002 during the first year of the ESSENCE project (Smith et al. 2002).

4.2.1. Keck-II + ESI

We obtained spectra of supernova candidates with ESI (Sheinis et al. 2002) on the Keck-II telescope during two separate observing runs in October and November of 2001. On all nights we used a $1.0''$ slit for the observations, with a spectral resolution of $\sim$1.4 Å. The slit was oriented along the parallactic angle, or to include either the nucleus of the host galaxy or a nearby bright star. Between integrations the target was moved along the slit to reduce the effects of fringing and increase confidence in identifying the SN spectrum. On October 21-22, the seeing was $0.6'' - 0.8''$. For November 16-18, the seeing was $0.5 - 0.6''$ on the first night and $0.7 - 0.8''$ on the final two nights. The standard stars BD+174708 and BD+284211 (Oke 1990) were used for flux calibration. Standard CCD processing and optimal spectral extraction were done with IRAF, with our own IDL routines used to calibrate the wavelengths and fluxes of spectra and to correct for telluric absorption bands.

We also obtained spectra with ESI on November 6, 2002, during ESSENCE project observations in order to measure additional redshifts of host galaxies. Seeing was $0.8'' - 0.9''$, and observational setup and reduction was the same as described for the 2001 nights.

4.2.2. Keck-I + LRIS

Additional spectra of SN candidates were obtained with LRIS (Oke et al. 1995) on the Keck-I telescope during two separate observing runs in December 2001 and January 2002. On December 22, the seeing was approximately $1''$, with high cirrus. On January 16-17, the seeing was $1.1 - 1.8''$ on the first night and $2 - 3''$ on the second night. We used a $1.0''$ slit for the observations. The spectral resolution is $\sim$6.2 Å for the red end (6500-10000 Å), and 9.2 Å for the blue (3300-6900 Å). Between integrations we moved the target along the slit for the reasons described above. In December standard star BD+174708 (Oke & Gunn 1983) was used for flux calibration, while in January standard stars BD+174708, BD+262606, and BD+284211 (Oke 1990) were used.

As with the ESI observations, we used IRAF for standard CCD processing and spectral extraction, and IDL for calibrating the wavelengths and fluxes of spectra and removing atmospheric absorption bands. We used the 300/5000 grism on the blue side over the range 3300-6900 Å, which was matched to the D680 dichroic. On the red side, we used the 400/8500 grating over the wavelength range 6500-10000 Å. Typically the two sides were tied together over the range 6500-6600 Å. There were any number of anomalies in the overlap range, which were minimized as much as possible, but some complications were unavoidable. Specific problems encountered included (1) second-order light on the blue side; (2) wavelength-dependent time variations in the dichroic; and (3) reflections from bright stars landing on targets on the blue side. We were able to work around the second-order blue light in our standard stars and ignore it in our objects (which are red). We also corrected for the variations in dichroic transmission to the red side, but not in the reflectance to the blue side. There is an increase in noise and possible spurious features exist near the overlap region.

4.2.3. VLT + FORS

We also obtained spectra of SN candidates with FORS1 on the VLT during an observing run on December 13 and 14 of 2001. On December 13, the seeing varied from $0.7''$ to $1.8''$. On December 14, the seeing changed rapidly from $\approx 0.7''$ to $1.3''$ until heavy clouds moved in mid-way through the night, so that most of the subsequent data did not have enough signal for analysis. We used a $1.0''$ slit for all observations, with a 300 line mm^{-1} grating. The slit was oriented to include the nucleus of the host galaxy. FORS1 is mounted behind an atmospheric dispersion compensator and we do not expect any wavelength dependent effect due to the setting of the slit at an angle different from the parallactic angle. Between integrations the target was moved along the slit to reduce the effects of fringing and for ease of identifying the SN spectrum. During the night of December 13 we observed EG21 and LTT 3218 as spectroscopic standards (Hamuy et al. 1992, 1994) at the beginning and end of the night, respectively.

The spectra were first corrected by bias subtraction and division by a dome flat. The wavelength scale was established through calibration observations of a HeCuAr lamp observed during the afternoons before and after the observations. The wavelength solution was then verified against night sky lines. The extraction of the spectra was carefully done to control the contamination by the underlying host galaxies. The spectra were then flux-calibrated using the sensitivity functions derived from the standard stars.

4.3. Supernova Classification

Type Ia supernovae are defined by the presence of Si II λ6355 and Ca II H+K $\lambda\lambda$3934, 3968, and typically show numerous broad undulations in their spectrum (see Filippenko 1997). For the redshifts targeted during this survey, the Si II line was not observable with visible spectroscopy, though we often could identify the Ca features, 4000 Å break, and other SN Ia features. Among the features that may be used to uniquely identify a SN Ia when Si II is not observed is the double-bump feature near 4000 Å created by the combination of Fe II λ4555 and Mg II λ4481. Typically the redshift was measured through host galaxy emission, most often the [O II] doublet at $\lambda\lambda$3726, 3729. This doublet is often unresolved by many instruments, and so appears as a single prominent feature, which in many cases could be interpreted as [O II] at high redshift, or Hα at low redshift. One means of distinguishing between these choices is the brightness of the host galaxy. Another is that Hα is likely to be accompanied by such lines as [N II], [S II], or [O III], so the lack of these other features indicates that [O II] is more likely. The ability to resolve this doublet will remove all doubt, and this was one advantage of using ESI, with its much greater resolving power compared to LRIS for spectroscopic observations (note the values for each instrument given above in Sections 4.2.1 and 4.2.2).

Supernovae were identified by matching spectral features with those of SNe Ia through a program called SNID (Tonry, in preparation), which cross-correlates an observed spectrum against a set of template spectra to determine the supernova type, redshift, and age. SNID uses a set of 171 template spectra which span a large range of SN Ia properties (a small number of templates for other types of supernovae are also used, though the diversity of SNe Ib/c and SNe II makes their usefulness more limited than for the relatively homogeneous SNe Ia). The best matches are reported in terms of a correlation value r. Comparisons at very different redshifts may require trimming the spectrum to varying degrees, and so SNID weights the correlation value by the amount of overlap between the spectrum and template (abbreviated *lap*), producing a parameter $r{*}lap$ which is used to determine which template matches are of highest significance.

Table 4 contains positions and galactic extinction values for 23 supernova candidates which we believe are truly SNe Ia, with spectroscopic observations described in Table 5 and images shown in Figures 3 and 4. Tables 6 and 7 give information on the redshift determination and SNID analyses, respectively. Nine objects are identified as unambiguous SNe Ia, meaning that they produce a strongly significant best-fit SNID correlation value at the same redshift as indicated by their host galaxy emission lines. The exception is SN 2002ad, for which the best SNID value is at $z \approx 0.77$, while the second most likely value is $z = 0.514$, which agrees with the host galaxy emission. However, the match at $z = 0.765$ is with a

template from just past maximum light, whereas the $z = 0.514$ match is at nearly two weeks past max, agreeing with the light curve. We therefore include SN 2002ad as an unambiguous SNe Ia at the host galaxy redshift. Spectral matches for these 9 SNe Ia as determined by SNID are shown in Figure 5. Note the presence of Si II λ6355 in SNe 2001iv and 2001iw, and evidence of the double peak at $\sim$4000 Å in the other seven SNe, indicating that these are indeed SNe Ia.

The remaining 14 objects are divided into two groups—11 with host galaxy redshifts which do not correspond to a strong SNID match, and 3 for which there is a significant SNID correlation with a SN Ia template but no host galaxy emission with which to compare. Of the group of 11, four (SNe 2001fo, 2001hs, 2002W, 2002X) have peak values of $r * lap > 3.0$, and so based purely on SNID correlation values appear to be as strong SN Ia candidates as SN 2002ad. The spectral matches are not convincing, however, and we are unwilling to accept these fits as significant (contamination of a spectrum by galaxy light often makes it impossible to clearly discern SN features, so they are still possible SNe Ia). One of the 11 objects (SN 2001jn) was observed in November 2002, long after the supernova had faded from view, so that a SNID analysis is not possible. The final group of 3 SNe (SNe 2001fs, 2001ix, 2001jm) do not possess visible host galaxy emission, but do produce convincing matches with template SNe Ia via SNID, as shown in Figure 6. However, SNID often produces a series of correlation peaks at discrete redshifts, due to successively matching different features in the spectrum of a SN Ia with alternate template features at different redshifts. Because of this ambiguity, we are unwilling to state purely on a spectroscopic basis that these objects are SNe Ia at the quoted redshift. Inspired by our substantial high-quality photometric information, we have pursued further investigations to determine whether they may be added to our sample with confidence that they are indeed SNe Ia.

A first test of these additional objects is to compare their photometric observations with what one would expect from various types of supernovae at the measured redshift. SNe Ia have been subjected to sufficient scrutiny in recent years that there is a good understanding of their general properties and a large number of well-observed objects. We have used two examples to demonstrate the breadth of parameter space that SNe Ia can be expected to cover—SN 1995D (Riess et al. 1999b) is a bright SNe Ia, with $\Delta = -0.42$ as measured by Riess et al. (1998), and $\Delta = -0.44$ from the MLCS method from this paper (see Section 5.1); SN 1999by is one the most subluminous SNe Ia ever observed (Garnavich et al. 2003). At redshift $z > 0.8$, objects such as SN 1999by will be too faint for detection at the $m \approx 24.3$ I-band sensitivity of our survey, but it can still serve as an illustrative limiting case for faint SNe Ia.

SNe II are more difficult because they are a less uniform population than SNe Ia (see Leibundgut & Suntzeff 2003). We have selected single spectroscopic observations of SN 1998S (Lentz et al. 2001; Leonard et al. 2000) and SN 1999em (Baron et al. 2000; Leonard et al. 2002) to serve as our templates. SN 1998S is a SN IIn which was observed at maximum brightness, and SN 1999em is a SN II-P which was also observed near maximum. These two objects can only begin to describe the vast diversity of SNe II, and were chosen primarily for their extensive spectral coverage into the UV.

These templates allow us to determine the expected photometric colors as a function of time for the various classifications of supernovae. Figure 7 shows $R-Z$ as a function of time relative to maximum brightness for 17 of the IfA Deep Survey SNe, divided into redshift bins of 0.1, from $z = 0.60 - 1.0$. Contours indicate the expected evolution of the two SNe Ia templates at these redshifts. For the SNe II, we calculated $R - Z$ boundaries of each redshift range for both of the templates, and inflated each color region by 0.15 magnitudes to allow for evolution as well as uncertainty in the true dispersion of the population. The times relative to maximum are calculated using light curve fits from Section 5.1 below.

The IfA Deep Survey supernovae, whether spectroscopically confirmed as SNe Ia or not, are all consistent with the contours predicted by the SN Ia templates. Many are not inconsistent with the SNe II contours as plotted, however, particularly those at very early times, as well as some at low redshift. For the very highest redshifts, the likely SNe Ia are all far too red by a week past maximum light to be consistent with SNe II. Also, as expected, at higher redshifts the SNe lie along the contours defined by the bright SN Ia 1995D, rather

than the subluminous SN 1999by.

These plots do not include contours for SNe Ib/c, due to the lack of suitable early-time templates in the UV. SNe Ib/c are typically much fainter than SNe Ia (with a luminosity function as given by Richardson et al. (2002) of M_B(Ib/c)=-18.04, compared to M_B(Ia)=-19.46), so we do not expect to be significantly contaminated at high redshift by these objects for the same reasons as for the faint SN Ia 1999by. However, SN Ic 1992ar (Clocchiatti et al. 2000) was potentially one of the brightest supernovae of any type ever observed, pointing out the risk in any argument based on the luminosity function. Richardson et al. (2002) further note that five of the eighteen SNe Ib/c in their sample (including SN 1992ar) are as bright or brigher than SNe Ia, possibly suggesting a bimodal distribution of faint and bright events.

Since these fourteen SNe are all consistent with SNe Ia at the appropriate redshift (although not necessarily inconsistent with other types of SNe), we have decided to continue to include them in our sample. In Section 5.1 we will mention a goodness-of-fit criterion which was used to further bolster our confidence in their inclusion. When we perform cosmological density parameter calculations in Section 6 below, we will do so using our entire sample of SNe discussed here, as well as with only the 9 unambiguous SNe Ia.

4.4. Discussion of IfA Deep Survey Yield

In Section 2, we noted that the IfA Deep Survey was expected to discover and monitor 10–25 SNe Ia in the redshift range of $0.9 < z < 1.2$. However, here we have reported only 4 such objects, with an additional 8 at slightly lower redshift ($0.8 < z < 0.9$). This raises a question that was the subject of much discussion even while the survey was still in progress: Why did we find so few SNe Ia at the highest redshifts?

The first possible answer is that we expected far too many objects due to overestimating the rates of SNe Ia at these redshifts. While it is possible that previous surveys with a lower sensitivity have overestimated the SNe rate at extremely high redshifts, there have been enough surveys (see Tonry et al. 2003) exploring out to high redshifts to indicate that our yield was unexpectedly and anomalously sparse. The continuous nature of the IfA Deep Survey, which has allowed us to augment our yield beyond those spectroscopically confirmed SNe Ia, means that we will be able to re-search the observations and potentially discover supernovae that may have been missed during the survey (for examples, SNe at the cores of galaxies may be misclassified as AGN). It will of course be impossible to obtain a supernova spectrum at this time, but in many cases we should be able to measure a host galaxy redshift, as was done with the November 2002 observation of SN 2001jn.

There are several additional potential explanations related to the details of the survey and its implementation. The first of these could be that our survey did not go as deep as we had initially expected. Another possible answer is that we did not do a complete job of discovering supernovae that were present in the observations. We did indeed discover $z \approx 1$ SNe Ia (objects at this flux level were not difficult to spot), as well as numerous other similar objects which were not spectroscopically confirmed, so we do not feel either of these explanations are correct. However, in any magnitude-limited survey a luminosity bias must be expected, so it may be that our sample is simply not complete to redshift $z \approx 1$ despite our expectations. There are also possible spectroscopic explanations analogous to the above speculations. For SNe at $z \approx 1$, at the extreme limits of what can be observed, good luck in both the timing and conditions of spectroscopic nights are crucial for successful observations. These concerns with both the photometric and spectroscopic observations illustrate the extreme difficulty in attempting large scale surveys for $z \approx 1$ SNe from the ground. Even with regular and frequent access to telescopes with the ability to detect such SNe, the vagaries of the atmosphere cannot be predicted in advance. And even when provided with advantageous weather, the exposure times required for spectroscopic confirmation mean that only a small fraction of discovered supernovae will be properly observed spectroscopically. The recent demonstration of the ACS grism on *HST* to obtain an identifiable spectrum of a $z = 1.3$ SNe Ia (Riess et al. 2003) shows the future of $z > 1$ supernova surveys is undoubtedly in space.

4.5. Supernova Light Curves

As discussed by Novicki & Tonry (2000) and Tonry et al. (2003), and expounded upon by Barris, Novicki, & Tonry (in preparation), we have developed a new method for calculating supernova light curves. The classic method for measuring SN fluxes is to obtain a template image, typically either at the start of a campaign (before the supernovae to be discovered have exploded) or at the end (often up to a year after the conclusion of the campaign, to ensure the supernova has faded completely), in which the supernova will not be present, so that the result of subtracting from an image of the supernova will yield the correct flux. If the template actually has a low level of supernova flux, the derived magnitudes will be incorrect. If it is necessary to wait up to a year to obtain a template image, there will be a significant delay in producing results. Furthermore, if this template image has poor seeing or low signal-to-noise, it will create large uncertainties in measured flux even if the supernova images themselves are of high quality.

Our new method, dubbed N(N-1)/2, collects all observations of a given supernova, subtracts every pair of images, and solves a corresponding matrix of flux differences. Novicki & Tonry (2000) demonstrated that this can lead to a decrease in uncertainties by a factor of $\sqrt{2}$, due to effectively using every image as a template, thus eliminating dependence upon a single exposure. Since there is no pre-defined zero-flux template in the N(N-1)/2 method, there is an ambiguity in the flux zero-point, which creates interesting issues for photometric fitting of SNe that are discussed more in Section 5.1.

The light curves for our 23 SNe as calculated via the N(N-1)/2 method are given in Table 8. These tables include the date of each observation and the measured flux of the supernovae, as well as information from the fits of the data, described below. All flux values are scaled so that flux=1 corresponds to $m = 25.0$, so that magnitudes may be calculated by

$$m = -2.5 \log(flux) + 25.0.$$

This is of course not properly defined for values of flux < 0, which indicate the lack of a detection in the given observation.

Uncertainties in magnitudes may be calculated directly from the uncertainties in flux according to the formula

$$\sigma(mag) = 2.5 \log(1 + \sigma(flux)/flux),$$

although these values will not be precise, as the uncertainties in magnitude are not symmetric due to the logarithm operation.

4.6. *HST* Photometric Observations

Our *HST* Cycle 10 allocation allowed us to obtain light curves of several supernovae with WFPC2 using the $F850LP$ filter. Since the IfA Deep Survey involved 5 different field positions, we could not predict in advance the location of the best supernova candidate(s) for each month. The Telescope Time Review Board approved our request to change our observations to Targets of Opportunity (ToO), which allowed us to pick the best supernova candidate, regardless of position.

After spectroscopically observing our candidates and confirming their identity as SNe Ia at a desirable redshift, selected objects were sent to *HST* for observation. The process of discovery, spectroscopic analysis, and notification to STScI of the ToO targets creates an unavoidable time gap of about 10–12 days between the discovery and the first *HST* observations. Typically, the discovery epoch of a high-z supernova is a few days before maximum brightness, and although the time dilation factor of $(1 + z)$ works to lessen the delay in the rest frame, none of our *HST* light curves begins until past maximum light. We observed SNe 2001hu, 2001jf, and SN 2001jh, with relevant information given in Table 9.

Each SN observational epoch consisted of approximately 3–5 orbits. The data were combined using the drizzle procedure outlined by Koekemoer et al. (2002). Determining accurate photometry from the WFPC2 images requires properly correcting for various CCD and optical effects, most importantly the non-unity charge transfer efficiency (CTE). We followed the procedure outlined by Dolphin (2000) in order to measure reliable PSF-fitting photometry. Along with the magnitude of the supernova, a few nearby stars were measured with the same photometric method. There were 5 epochs for SN 2001jh and 6 each for SNe 2001hu and 2001jf, so the same stars were measured several times with consistent results.

We also obtained ACS images well after the completion of the survey to serve as templates in order to subtract in the same manner as for the ground-based observations. These subtractions were not done using the N(N-1)/2 method, but rather used the classic single-template method. This was done for the sake of simplicity, but should be acceptable since none of the problems associated with the single-template method is an issue (poor seeing, S/N, or timing of the template).

5. Distance Determination

5.1. The Multi-wavelength Light Curve Shape Method

In order to use these SNe Ia for cosmological analysis, we created a new version of the Multi-wavelength Light Curve Shape (MLCS) analysis method (see Riess, Press, & Kirshner (1996, hereafter RPK96), and Jha 2002). This new implementation was developed in consultation with authors of previous versions of the MLCS fitting code, and features few substantial changes from them. The MLCS method simultaneously fits for distance modulus ($m-M$), A_V, and Δ, a parameter defined by the difference in absolute magnitude between a given supernova and a fiducial SN Ia. This Δ parameter therefore describes the shape of the SN light curve, since there is a correlation between absolute magnitude and light curve shape (see Phillips 1993).

We first constructed MLCS templates through iteratively fitting a sample of 32 low-z SNe Ia taken from the Calán/Tololo survey (Hamuy et al. 1996), as well as from Riess et al. (1999b) and Jha (2002). At the end of this training process the fits to these 32 SNe Ia produced a scatter of 0.14 magnitudes around the Hubble Diagram.

K-corrections were calculated using the formulae described in Kim, Goobar, & Perlmutter (1996) and Schmidt et al. (1998), using a set of 135 SN Ia spectra ranging from 14 days before maximum light to 92 days after maximum light. As described by Nugent, Kim, & Perlmutter (2002) as well as Germany et al. (2003), before applying the K-correction formulae, the SN Ia spectra are first matched to the $B-V$ color of the MLCS template by applying the Savage-Mathis (1979) reddening law. The Schlegel, Finkbeiner, & Davis (1998, hereafter SFD) galactic extinction is applied to the Ia spectra set, and the spectra are then stretched by the appropriate factor of $(1+z)$. These modified spectra are used to calculate the K-correction, providing a series of K-correction estimates as a function of SN age, which is fit with a 3-knot spline. The resulting K-corrections are interpolated from this spline, and the uncertainty in the K-corrections estimated from the scatter about the fitted relationship. These K-corrections are then used to fit the best template (which has its own $B-V$ evolution based on its intrinsic colour and fitted extinction), with this new $B-V$ evolution used in place of the MLCS template, and the subsequent steps repeated until convergence is reached. Typically, this iterative process changes the K-corrections by <0.03 mag.

Calculating proper K-corrections depends upon knowing the shape of the light curve (i.e. the MLCS Δ parameter) as well as the reddening of the supernova spectrum (A_V). Thus in the fitting procedure we were forced to select given input values for Δ and A_V, determine the necessary K-corrections for such a light curve shape, and then fit for the best output set of parameters. If the best-fit values of Δ and A_V were equal to the input values (a rigid constraint of within 0.01 for each parameter was used), then the solution was deemed acceptable. During the fit procedure, the constraint that $A_V > 0$ was applied, rather than allowing for a solution with negative extinction. This eliminates the need to apply a Bayesian prior after the fact (as done by RPK96), which affects A_V while leaving untouched the other, correlated, parameters $(m-M)$ and Δ.

For each MLCS run on a supernova, the appropriate SFD galactic extinction is applied to the light curve (for the Z filter used here, we calculated a value of A/E_{B-V} of 1.520 following the description from SFD), the points are shifted so that $t=0$ at $t=t_0$, and the time dilation factor of $(1+z)$ applied. For high-redshift objects ($z>0.7$), we K-corrected I band to B, and Z to V, to match with the filters we had used to train the MLCS method. For SNe 2001hu, 2001jf, and 2001jh we also K-corrected $F850LP$ to V. For low-redshift objects ($z<0.7$) we shifted R and I bands to B and V, respectively. Tables 8 and 9 include K-correction values for the filters used in MLCS fitting. Our MLCS templates extended from 10 days prior to maximum light in the rest

frame to 40 days post-maximum. The reason for this late-time cutoff was that the templates were created with this survey in mind, and so were tailored for SNe Ia at $z \approx 1.0$, which will fade from visibility by this point in the light curve, rather than for lower redshift objects, which will still be visible. The early-time cutoff is due to the paucity of low-z supernova observations at earlier epochs for constructing MLCS templates. However, we have extended our fits to earlier times using a prescription similar to that of Riess et al. (1999a), with a slight modification to account for zero-point differences. This extension allows us to take advantage of the unprecedented number of very early light curve points provided by the continuous nature of the survey.

The use of the N(N-1)/2 method for producing light curves did lead to some complications in the light curve analysis due to the ambiguity concerning the flux zero point. The proper way to account for this is to recognize that the flux zero point is in fact a free parameter, and fit for it accordingly. Thus, our MLCS code, in addition to fitting for the time of maximum t_0 (externally, through iteration), distance modulus $(m - M)$, extinction A_V, and MLCS delta parameter Δ (constrained to lie between $-0.6 < \Delta < +0.6$), also fits for offsets in each filter, δ_B and δ_V. These offsets are done in flux, not magnitude, since these are flux differences rather than a multiplicative factor.

A further constraint was placed on satisfactory values of δ_B and δ_V. We can ascertain that our zero points are roughly reliable since our time baseline is long enough that, in practice, there is always an observation with little or no supernova flux. Because of our confidence in the general accuracy of our flux zero point, we only accept solutions with small values for δ_B and δ_V. Also, for SNe 2001hu, 2001jf, and 2001jh, we did not fit for a flux offset for the $F850LP$ points, as these magnitudes were calculated using the single-template method.

Best-fit MLCS parameters ($m - M$, A_V, Δ) for the IfA Deep Survey SNe Ia are given in Table 10. Table 8 includes the values for time relative to B band maximum in the supernova rest frame for every observation. Uncertainties in the parameters ($m - M$, A_V, Δ) were calculated in the same way as given in RPK96. Light curves with MLCS fits are shown in Figure 8 for the 9 spectroscopically confirmed SNe Ia and Figure 7 for the 14 additional SNe Ia. In these figures, we have plotted the flux values for all SNe scaled so that $magnitude = 25$ corresponds to a value of $flux = 1$.

We have also included in Table 10 the χ^2/N values for the MLCS fits for all 23 SNe. The fits are quite good for all of the SNe Ia, both spectroscopically confirmed with SNID and otherwise. These χ^2/N values for the 14 likely SNe Ia lend further confidence to their identification as SNe Ia and inclusion in our sample.

5.2. Additional Fitting Methods

In addition to MLCS fits, we also analyzed the SN Ia light curves with the Bayesian Adapted Template Match (BATM) Method (Tonry, in preparation) and dm15 (Germany 2001). BATM uses a set of approximately 20 well observed nearby supernova light curves in combination with ∼100 observed spectral energy distributions (SEDs) in an attempt to span the expected behavior of SNe Ia. For all pairs of light curve and SED, BATM calculates likelihoods as a function of distance d, extinction A_V, and time of explosion t_0, further marginalizing over t_0 and applying a prior on A_V as described by Tonry et al. (2003), in order to measure d and A_V. The dm15 method is a modification of the Δm_{15} method of Phillips et al. (1999), which utilizes the facts that the decline in magnitudes of SNe Ia in the first 15 days after B-band maximum light correlates with luminosity, and that the late-time color curves of all unreddened SNe Ia are uniform, regardless of decline rate (Lira 1995; however, the peculiar SN Ia 2002cx (Li et al. 2001), does not follow the standard Lira relation). In the dm15 method, a set of 15 template light curves of nearby SNe Ia is used to measure distance d, marginalizing over t_0 and A_V for each template with an acceptable fit.

Results of light curve fits for the IfA Deep Survey SNe Ia from each of these two methods are given in Table 11 (The dm15 method was not used for SNe at $z > 0.8$ due to the lack of observed filters to match its templates). The three methods are all quite consistent with each other, with scatter between each pair of methods of ∼0.1 magnitudes. We have also combined all our measurements into a single value for distance in the same manner as Tonry et al. (2003). Zero-point dif-

ferences between each method were computed by comparing common SN measurements, distances placed on a Hubble flow zero-point (dH_0), and the median selected as the best distance estimate. Uncertainty in the distance estimate was taken from the median of the error estimates from the individual methods, scaled down by the 1/4 power of the number of contributors. As described by Tonry et al., this median procedure is not expected to significantly improve the accuracy of the final estimate, but ideally will result in a more Gaussian-like distribution. Supernova properties derived by combining results from all the methods are included in Table 12 in a form designed to be similar to those given by the summation of Tonry et al. (2003).

6. Cosmology with IfA Deep Survey Supernova

Tonry et al. (2003) collected redshifts and distances for all published SNe Ia at cosmological distances. Whenever possible, they also performed various light curve fits to the published photometry in order to place as many as possible on a common system. They present redshift and luminosity distance for a total of 230 SNe Ia. However, this includes many objects which may be unsuitable for cosmological analysis, particularly those which are heavily extinguished or are nearby enough for velocity uncertainties to be a major problem.

The results from the distance fits from the previous section are illustrated on a Hubble diagram in Figure 10, which includes all of our SNe Ia, as well as those from Tonry et al. (2003). These figures show the result of subtracting the distance modulus predicted from an "empty universe," i.e. a cosmology with $(\Omega_M, \Omega_\Lambda)$=(0.0, 0.0), from that measured for each supernova. Although the distances given in Tables 10 and 11 are in the form of $(m-M)$ for the sake of familiarity, to construct the figures we only need use the values from Table 12, which have no dependence on H_0. Immediately obvious on the plot is the large number of literature points at $z \approx 0.5$ with a positive deviation, which is the signature of an accelerating universe and a cosmological constant-like term. Supernova surveys targeting $z \approx 0.5$ were well placed to detect the presence of Ω_Λ. A survey for supernovae at $z = 1.0$, on the other hand, is designed to target the redshift region where the deviation between a Ω_Λ-dominated universe and a systematic effect proportional to redshift is large. This was the goal of the IfA Deep Survey, though it turned out that we discovered supernovae over a fairly large range in redshift, and many fewer than expected at $z \approx 1$, as was discussed in Section 4.4. Nevertheless, the number of $z \geq 0.7$ SNe (15, see Table 12) which the IfA Deep Survey has added to what was heretofore an extremely sparse region of redshift space is still substantial, doubling previously published results (12 from the collection presented by Tonry et al. 2003, plus 3 from Knop et al. 2003 which are not included in this analysis).

We have also taken medians by redshift bins in order to better illustrate the overall trend with redshift, using the subset of 200 literature SNe with $A_V \leq 0.5$ plus 22 from this survey, and requiring that bins must have a width of at least 0.25 in log z, and contain at least 20 SNe. Results are shown in Figure 11. Our new SNe have continued to fill in the highest redshift bins, and show an even more rapid and sharp turnover than was observed by Tonry et al. The median magnitude deviation relative to an empty universe for the highest-z bin, calculated as 0.00 magnitudes in Tonry et al. for 12 objects centered at $z = 0.87$, is now -0.07 magnitudes for 20 objects centered at $z = 0.89$, while the uncertainty in this bin, estimated by the 68% scatter of points in the bin, is 0.07 mags compared to 0.08 mags from the Tonry et al. sample. These changes are due to the fact that the SNe at $z > 0.85$, which are predominantly from this survey, are overwhelmingly *brighter* than the empty-universe cosmology, compared to those at slightly lower redshift which tend to be fainter than this model. Although the region at $z \approx 1$ is still underpopulated, it is becoming more and more apparent from the sample presented here that the trend of the population of SNe Ia at $z > 0.5$ is more consistent with the turnover predicted by an Ω_Λ-dominated cosmology rather than a systematic effect which increases with redshift (see Figure 11).

6.1. Cosmological Density Parameter Determination

We now turn to determination of cosmological density parameters from the supernova data. We wish to calculate χ^2 as a function of the pa-

rameters $(H_0, \Omega_M, \Omega_\Lambda)$. Since we have SN Ia distances over a wide range of redshift, we are able to marginalize over H_0 and concentrate solely on the Ω parameters. H_0 appears as a quadratic term in χ^2, as shown below, so it appears as a separable Gaussian factor in the probability to be marginalized over, and doing so over H_0 is equivalent to evaluating χ^2 at its minimum with respect to H_0.

The distance modulus for the observations may be rewritten as

$$(m-M)_{obs} = 5\langle \log(dH_0)\rangle + 25 - 5\ \log H_{0,1}.$$

For a given cosmology, the luminosity distance can be expressed as

$$d_{lum} = f(z, \Omega_M, \Omega_\Lambda)/H_{0,2}.$$

Therefore

$$(m-M)_{model} = 5\ \log f + 25 - 5\ \log H_{0,2},$$

where the Hubble parameter $H_{0,2}$ used for calculating the model is not necessarily equal to that used for the observational data ($H_{0,1}$). This would not be by choice, but rather reflects the fact that the distances presented by Tonry et al. (2003), which are tied to the Hubble flow, are related to the "true" H_0 only by a fit parameter and therefore any new fit of distance must revisit this parameter, necessitating marginalization over H_0.

Calculating χ^2 is simply the sum over all supernovae

$$\chi^2 = \sum \frac{((m-M)_{obs} - (m-M)_{model})^2}{\sigma(\langle \log(dH_0)\rangle)^2}$$

$$\chi^2 = \sum \frac{(5\langle \log(dH_0)\rangle - 5\ \log f + 5\ \log(H_{0,2}/H_{0,1}))^2}{\sigma(\langle \log(dH_0)\rangle)^2}$$

where, as in Tonry et al. (2003), we also add a 500 km sec^{-1} uncertainty in quadrature to the redshift errors given therein to account for uncertainties due to peculiar motions.

For any cosmology $(\Omega_M, \Omega_\Lambda; z)$, f is a given, and the ratio $H_{0,2}/H_{0,1}$ is an unknown parameter on which χ^2 depends. The minimum value of χ^2 occurs where this parameter has the value

$$log(H_{0,2}/H_{0,1})_{min} = -\frac{\sum \frac{5\langle \log(dH_0)\rangle - 5\ \log f}{\sigma(\langle \log(dH_0)\rangle)^2}}{\sum \frac{1}{\sigma(\langle \log(dH_0)\rangle)^2}}.$$

We then convert to a probability value proportional to $\exp(-0.5\chi^2)$, with χ^2 evaluated at this minimum, which allows us to determine contours of constant probability density for (Ω_m, Ω_Λ).

We can now add our new high-redshift supernovae to the previously published SNe and investigate the implications for cosmology. For determination of cosmological parameters, Tonry et al. (2003) used cutoffs of $z > 0.01$ and $A_V \leq 0.5$, and we have chosen to adopt the same restrictions, leaving a sample of 172 objects. A first test is to calculate cosmological parameter best-fit regions using only the IfA Deep Survey SNe. The low-z dataset is crucial to constrain the Hubble constant, so we include objects with $z \leq 0.30$, but no objects at higher redshift save the 22 IfA Deep Survey SNe with $A_V \leq 0.5$ (eliminating SN 2001jn, as seen by Table 12). This reduces the sample size to 98 from the compilation by Tonry et al. (2003) and 22 from this study, for a total of 120 objects. With these 120 SNe Ia, we obtain a best-fit value of χ^2=97.7 at (Ω_m, Ω_Λ)=(0.27, 0.36). Corresponding probability contours derived from this sample are shown in Figure 12a. The best-fit value with $\Omega_{total} = 1.0$ (consistent with measurements of the cosmic microwave background (CMB), see below), is (Ω_m, Ω_Λ)=(0.42, 0.58). If we further restrict our high-z sample to only those 9 SNe Ia for which we obtained unambiguous spectral SN Ia confirmation, for a total set of 107, the minimum value of χ^2=85.2 occurs at (Ω_m, Ω_Λ)=(0.09, 0.15) (see Figure 12b). The fact that χ^2/N is much less than 1 is due to the 98 SNe Ia at $z \leq 0.30$, whose contribution to χ^2 for an empty-universe is 77.3. The 9 IfA Deep Survey SNe identified as SNe Ia by SNID contribute approximately 8 units of χ^2, with the additional 13 SNe Ia contributing approximately 12 units, indicating both that there is no sign of a difference in the distributions of the two subsamples as might be feared if there were incorrectly identified SNe Ia in the latter, and that our distance uncertainties are reasonable.

The fact that the IfA Deep Survey SNe agree well with an empty-universe cosmology is to be expected based on their redshift distribution. As is seen by the models plotted in Figure 10, in the redshift range $z = 0.8 - -1.0$ the difference between an Ω_Λ-dominated universe and an empty-universe is decreasing, meaning there is little power to differentiate between these models

from such SNe.

Adding our 22 SNe Ia to the full Tonry et al. dataset of 172 objects and following the same procedure, we obtain the contours shown in Figure 12c. The best-fit value is χ^2=195.5 at (Ω_m, Ω_Λ)=(0.71, 1.28). These contours are quite similar to those obtained by Tonry et al., who found a best fit at (Ω_m, Ω_Λ)=(0.69, 1.34), which is to be expected since the new data are statistically compatible with the Tonry et al. set. If we add the constraint that $\Omega_{total} = 1.0$, we obtain a best-fit at (Ω_m, Ω_Λ)=(0.33, 0.67). It is interesting to note, as did Tonry et al., that the supernova results intersect the line $\Omega_{total} = 1.0$ at the point which is also consistent with constraints from the 2dF survey of $\Omega_M h = 0.20 \pm 0.03$.

The best-fit value for the sample of 194 SNe Ia, however, is far from the $\Omega_{total} = 1.0$ line, although it is consistent with such values. The IfA Deep Survey SNe contours, while larger due to smaller sample size, are centered closer to this line. The majority of objects at $z \approx 0.5$ lie *above* the (Ω_m, Ω_Λ)=(0.3, 0.7) model, pushing Ω_Λ higher, while those at $z > 0.7$ mostly lie *below* the line, which pushes Ω_M higher in order to compensate, moving the contours into the region seen in Figure 12c. The reason can be seen from the median values given in Figure 11, where the population of SNe at z≈0.4-0.6 becomes fainter than those at lower redshift, only to have an extreme drop again for the highest redshift bin. These subsamples are drawn from many different sources, and within any previous study there was often a very heterogeneous mix of observations. For example, the light curves presented by Tonry et al. (2003) were obtained on as many as 6 different telescope/instrument combinations, even within a single filter, introducing many possibilities for photometric errors. By contrast, the uniformity of the observations and reductions of the IfA Deep Survey should minimize such possible sources of bias, while still subject to systematic errors such as uncertainties in K-corrections. Another possible source of systematic errors involve our dependence on the Z filter, whose photometry is ill-defined compared to other filters.

We can also explore the possible effects of gravitational lensing on our results. In order to do so, we perform the above calculations with Dyer-Roeder (DR) distance formulae (Fukugita et al. 1992; see also Dyer & Roeder 1972, 1973), which allow for the fact that the space through which light is propagating is inhomogeneous. In the above calculations, we have used the standard Robertson-Walker metric, which treats the distribution of material in the universe as being completely smooth. Depending on the true distribution, this may introduce errors in our cosmological parameter determination, as demonstrated by Kantowski (1998). An alternative model to consider is one in which light from the supernovae travels along a path entirely devoid of matter, hence the term "empty beam," in contrast to "filled beam" for the standard model. There are also intermediate possibilities to consider, though we will limit ourselves to the empty-beam alternative.

As shown by Holz (1998), an empty-beam model tends towards higher values of Ω_m and lower values of Ω_Λ. The likelihood contours also become greatly elongated, particularly towards higher values of Ω_m. This effect is seen in the comparison of our contours from Figure 12c and those from an empty-beam calculation, shown in figure 12d. Although these contours extend to extremely large values of (Ω_m, Ω_Λ), it is clear that adopting the empty-beam model still requires a non-zero value of Ω_Λ.

However, there is also the potential for magnification due to gravitational lensing to affect our results. The probability for significant magnification of sources at $z \approx 1$ are low (see Barber et al. 2000), but when combined with potential systematic effects, such as a selection bias for such brightened objects, could become important and partially account for the distribution of our $z > 0.8$ SNe Ia, which lie brighter than the favored (Ω_m, Ω_Λ)=(0.3, 0.7) model.

6.2. Comparison with WMAP

Recent results from high angular resolution observations of the CMB with WMAP (Spergel et al. 2003) have produced extremely tight regions of acceptable cosmological parameters which we can compare with our derived values. They find that the universe is consistent with being flat ($\Omega_{total} = 1.02 \pm 0.02$). All plots in Figure 12 indicate the line $\Omega_{total} = 1.0$. As was noted in the previous section, the 1-σ uncertainties for the full set of 194 SNe Ia no longer overlap with this line.

The contours from the IfA Deep Survey are larger, since they are based on a smaller sample, but are centered at values in better agreement with those preferred by the CMB. As mentioned above, it is expected that the best-fit contours for our SNe should lie closer than the full literature sample to an empty-universe model, based on redshift distribution, though the improved agreement with the CMB may also be due to the homogeneous nature of our sample minimizing systematic effects, which would bode well for future large-scale surveys which will have similar (though much larger) datasets.

7. Conclusion

We have described in detail the observational strategy and data reduction of the IfA Deep Survey as undertaken by a collaboration of IfA astronomers in late 2001 and early 2002, as well as the supernova search component carried out by the High-z Supernova Search Team. This survey has already served as an unprecedented photometric dataset for continuous detection and follow-up of high redshift supernovae, of which over 100 candidates were discovered (Barris et al. 2001, 2002), including the 23 SNe presented here. Preliminary analysis of survey data has also already yielded numerous substellar objects (Liu et al. 2002; Graham 2002; Martín et al., in preparation), indicating that large numbers of such objects will be discovered with more detailed inspection of the data. Similarly, the photometric dataset produced by this survey has great promise for many areas of research such as AGN studies, galactic structure, and galaxy clustering. The survey also anticipates even more ambitious future projects which will repeatedly image large patches of sky over extended periods of time, such as PanSTARRS, LSST, and the proposed SNAP.

These 23 SNe include 15 which double the previously published sample size of $z > 0.7$ supernovae. This region of redshift space is extremely important for distinguishing between systematic effects and cosmological evolution. These supernovae, in combination with the published body of SNe Ia, do not show evidence for continuing to grow ever fainter at higher values of z, as would be expected by a systematic effect proportional to redshift (see Figures 10 and 11). We have performed cosmological density parameter fits using different subsets of the 23 SNe—the sample of 9 objects which are unambiguously spectroscopically identified as SNe Ia, and the sample of 22 which have $A_V \leq 0.5$ (see Table 12). Both samples are consistent with the geometrically flat universe preferred by studies of the CMB (Figure 12). With the constraint of $\Omega_{total} = 1.0$, we obtain a best-fit at (Ω_m, Ω_Λ)=(0.33, 0.67) using our set of 22 and the literature collection presented by Tonry et al. (2003). Future studies which will produce similarly homogeneous datasets on an even larger scale may continue to show better agreement with the CMB and other constraints on cosmological density parameters, as our subsample does compared to the full literature sample.

Our yield, though impressive, was smaller than anticipated, demonstrating the difficulty of successfully finding SNe Ia at z≈1 and higher from the ground, even with a well-planned and executed survey using some of the world's largest telescopes. Spectroscopic resources in particular continue to be a strongly limiting factor for such supernova surveys. To collect much larger numbers of these supernovae in a reasonable time period will certainly require leaving behind operations from the ground.

We thank the staffs at all the observatories involved for their assistance with observations. We also thank the referee, David Branch, for many helpful comments on the manuscript. Partial support for this work was provided by NASA grants GO-08641 and GO-09118 from the Space Telescope Science Institute, which is operated by AURA, Inc., under NASA contract NAS5-26555. Funding was also provided by NSF grant AST-0206329. STH acknowledges support from the NASA LTSA grant NAG5–9364.

REFERENCES

Alard, C., 2000, AAPS, 144, 363

Alard, C., & Lupton, R.H. 1998, ApJ, 503, 325

Barber, A.J., et al. 2000, MNRAS, 319, 267

Baron, E., et al. 2000, ApJ, 545, 444

Barris, B., et al. 2001, IAU Circ. 7745, 7755, 7767, 7768

Barris, B., et al. 2002, IAU Circ. 7801, 7802, 7805, 7806, 7849

Benitéz, N., et al.2002, ApJL, 577, 1

Blakeslee, J.P., et al. 2003, astro-ph/0302402

Ciliegi, P., et al. 2003, A&A, 398, 901

Clocchiatti, A., et al. 2000, ApJ, 529, 661

Coil, A.L., et al. 2000, ApJ, 544, 111

Cuillandre, J-C., et al. 1999, CFH Bull. 40

de Ruiter, H.R., et al. 1997, A&A, 319, 7

Dolphin, A. E. 2000, PASP, 112, 1383

Dyer, C.C., & Roeder, R.C. 1972, ApJ, 174, L115

Dyer, C.C., & Roeder, R.C. 1973, ApJ, 180, L31

Fadda, D., et al. 2002, A&A, 383, 838

Filippenko, A.V. 1997, ARA&A, 35, 209

Ford, H.C., et al. 1998, Proc. SPIE, 3356, 234

Freedman, W.L., et al. 2001, ApJ, 553, 47

Fukugita, M., et al. 1992, ApJ, 393, 3

Fukugita, M., et al. 1996, AJ, 111, 1748

Garnavich, P.M., et al. 2003, in press (astro-ph/0105490)

Germany, L.M. 2001, PhD. Thesis, Australian National University

Germany, L.M., et al. 2003, A&A, in press

Giavalisco, M., et al. 2002, IAU Circ. 7981

Glazebrook, K., et al. MNRAS, 273, 157.

Graham, M. 2002, BAAS, 34, 1175

Hamuy, M., et al. 1992, PASP, 104, 533

Hamuy, M., et al. 1994, PASP, 106, 566

Hamuy, M., et al. 1996, AJ, 112, 2408

Hasinger, G., et al. 1993, A&A, 275, 1

Holz, D.E. 1998, ApJ, 506, L1

Jha, S. 2002, PhD. Thesis, Harvard University

Kaiser, N., et al. 1999, astro-ph/9907229

Kaiser, N. 2000, ApJ, 537, 555

Kaiser, N., Pan-STARRS Team. 2002, BAAS, 34, 1304

Kantowski, R. 1998, ApJ, 507, 483

Kim, A., Goobar, A., & Perlmutter, S. 1996, PASP, 108, 190

Knop, R.A., et al. 2003, astro-ph/0309368

Koekemoer, A.M., et al. 2002, *HST Dither Handbook*

Landolt, A.U. 1992, AJ, 104, 340

Leibundgut, B. 2001, ARA&A, 39, 67

Leibundgut, B., & Suntzeff, N.B. 2003, in *Supernovae and Gamma−Ray Bursts*, ed. K. Weiler, Heidelberg: Springer, 76

Lentz, E.J., et al. 2001, ApJ, 547, 406

Leonard, D.C, et al. 2000, ApJL, 536, 239

Leonard, D.C., et al. 2002, PASP, 114, 35

Li, W., et al. 2001, PASP, 113, 1178

Lilly, S.J., et al. 1995, ApJ, 455, 50.

Lira, P. Master's thesis, Univ. of Chile

Liu, M., et al. 2002, ApJ, 568, L107

Lockman, F.J., Jahoda, K., & McCammon, D. 1986, ApJ, 302, 432

Miknaitis, G., et al. 2002, BAAS, 34, 1205

Miyazaki, S., et al. 1998, in Proc. SPIE, 3355, 363

Mon et, D. 1998, http://archive.eso.org/skycat/servers/usnoa

Novicki, M.C., & Tonry, J. 2000, BAAS, 32, 1576

Nugent, P. 2001, in Particle Physics and Cosmology: Second Tropical Workshop, ed. J.F. Nieves (New York: AIP), 263

Nugent, P., Kim, A., & Perlmutter, S. 2002, PASP, 114, 803

Oke, J.B., 1990, AJ, 99, 1621

Oke, J.B., & Gunn, J.E. 1983, ApJ, 266, 713

Oke, J.B., et al. 1995, PASP, 107, 375

Pain, R., et al. 1996, ApJ, 473, 356

Pain, R., et al. 2002, ApJ, 577, 120

Percival, W.J., et al. 2001, MNRAS, 327, 1297

Perlmutter, S., et al. 1999, ApJ, 517, 565

Phillips, M., 1993, ApJL, 413, 105

Phillips, M.M., et al. 1999, AJ, 118, 1766

Postman, M., et al. 1998, ApJ, 506, 33

Poznanski, D., et al. 2003, PASP, 114, 833

Richardson, D., et al. 2002, AJ, 123, 745

Riess, A.G., Press, W.H., & Kirshner, R.P. 1996, ApJ, 473, 88

Riess, A.G., et al. 1998, AJ, 116, 1009

Riess, A.G., et al. 1999a, AJ, 118, 2675

Riess, A.G., et al. 1999b, AJ, 117, 707

Riess, A.G., et al. 2000, ApJ, 536, 62

Riess, A.G., et al. 2001, ApJ, 560, 49

Riess, A.G. 2002, BAAS, 201, 3901

Riess, A.G., et al. 2003, ApJL, in press (astro-ph/0308185)

Savage, B.D., & Mathis, J.S. 1979, ARA&A, 17, 73

Schlegel, D.J., Finkbeiner, D.P., & Davis, M. 1998, ApJ, 500, 525

Schmidt, B.P., et al. 1998, ApJ, 507, 46

Sheinis, A.I., et al. 2002, PASP, 114, 851

Smith, R.C., et al. 2002, BAAS, 34, 1232

Spergel, D.N., et al. 2003, ApJS, 148, 175

Stoughton, C., et al. 2002, AJ, 123, 485

Sullivan, M., et al. 2003, MNRAS, 340, 1057

Suntzeff, N.B., et al. 2003, in prep

Taniguchi, Y., Kawara, K., & Matsuhara, H. 1999, Ap&SS, 266, 313

Tonry, J.L., et al. 2003, ApJ, 594, 1

Williams, B.F., et al. 2003, ApJ, submitted

Williams, R.E., et al. 1996, AJ, 112, 1335

Wittman, D., et al. 2002, SPIE, 4836, 73

York, D.G., et al. 2000, AJ, 120, 1579

This 2-column preprint was prepared with the AAS LaTeX macros v5.0.

TABLE 1
TARGET FIELD CENTRAL COORDINATES

Telescope	Field Name	R.A.[1](2000)	Declination[2](2000)
CFHT	0230	02:27:53	+00:35:00
CFHT	0438	04:38:40	–01:30:00
CFHT	0749	07:49:55	+10:09:00
CFHT	0848	08:48:30	+44:15:00
CFHT	1052	10:52:20	+57:20:00
Subaru	0230E	02:28:46	+00:35:00
Subaru	0230W	02:27:00	+00:35:00
Subaru	0438E	04:39:33	–01:30:00
Subaru	0438W	04:37:47	–01:30:00
Subaru	0749E	07:50:48	+10:09:00
Subaru	0749W	07:49:02	+10:09:00
Subaru	0848E	08:49:43	+44:15:00
Subaru	0848W	08:47:17	+44:15:00
Subaru	1052N	10:52:20	+57:33:09
Subaru	1052S	10:52:20	+57:06:51

[1]hh:mm:ss

[2]dd:mm:ss

TABLE 2
CFHT+12K SCIENCE OBSERVATIONS

date	MJD	field	I[1]	FWHM[2]
Sep 11	52163.54	0230	8×600	0.72
Sep 24	52174.56	0230	8×600	0.68
Oct 9	52191.43	0230	8×600	0.69
Nov 12	52225.31	0230	8×600	0.66
Dec 18	52263.23	0230	10×600	1.06
total		0230	25200s	
Sep 12	52164.57	0438	8×600	0.75
Sep 24	52176.49	0438	8×600	0.72
Oct 9	52191.50	0438	8×600	0.71
Nov 12	52225.39	0438	8×600	0.62
Dec 18	52263.38	0438	8×600	1.14
total		0438	24000s	
Oct 13	52195.57	0749	8×600	0.77
Nov 12	52225.48	0749	8×600	0.77
Dec 18	52262.50	0749	8×600	0.80
total		0749	14400s	
Oct 9	52191.56	0848	8×600	0.78
Nov 12	52225.56	0848	8×600	0.77
Dec 18	52263.51	0848	8×600	1.42
total		0848	14400s	
Dec 18	52263.57	1052	8×600	1.13
total		1052	4800s	

[1]All exposure times in seconds.

[2]arcseconds

TABLE 3
SUPRIME-CAM SCIENCE OBSERVATIONS

date	MJD	field	R[1]	I[1]	Z[1]	field	R[1]	I[1]	Z[1]	FWHM[2]
Oct 16	52198.47	0230E	...	3×215	5×240	0230W	...	3×215	5×240	0.64
Oct 22	52204.46	0230E	2×280	3×215	5×240	0230W	2×280	3×215	5×240	0.66
Nov 18	52231.43	0230E	2×280	3×215	5×240	0230W	2×280	3×215	5×240	0.63
Nov 19	52232.26	0230E	3×280	3×215	5×240	0230W	2×280	3×215	5×240	0.64
Nov 23	52236.24	0230E	2×280	3×215	4×240	0230W	2×280	3×215	4×240	0.95
Dec 9	52252.24	0230E	2×280	3×215	5×240	0230W	2×280	3×215	5×240	0.94
Jan 9	52283.31	0230E	2×280	3×215	5×240	0230W	2×280	3×215	4×240	0.60
Jan 14	52288.30	0230E	2×280	3×215	5×240	0230W	2×280	3×215	5×240	0.70
Jan 15	52289.32	0230E	2×280	3×215	2×240,	0230W	2×280	3×215	5×180	1.02
			...	...	3×180					
Feb 17	52323.25	0230E	...	3×215	3×240	0230W	...	3×215	3×240	1.07
total		0230E	4760	6450	11100	0230W	4480	6450	10740	
Oct 16	52198.55	0438E	...	3×215	5×240	0438W	...	4×215	5×240	0.69
Oct 22	52204.56	0438E	2×280	3×215	5×240	0438W	2×280	4×215	5×240	0.67
Nov 18	52231.39	0438E	3×280	3×215	5×240	0438W	2×280	3×215	5×240	0.63
Nov 19	52232.37	0438E	2×280	3×215	5×240	0438W	2×280	3×215	5×240	0.74
Nov 23	52236.34	0438E	2×280	3×215	4×240	0438W	2×280	3×215	4×240	0.89
Dec 9	52252.34	0438E	2×280	3×215	5×240	0438W	2×280	3×215	5×240	0.88
Jan 9	52283.40	0438E	2×280	3×215	3×240	0438W	2×280	3×215	3×240	0.63
Jan 14	52288.26	0438E	2×280	3×215	5×240	0438W	2×280	3×215	3×240	0.81
Jan 15	52289.30	0438E	2×280	3×215	5×240	0438W	2×280	3×215	5×240	0.82
Feb 17	52323.33	0438E	1×280	3×215	5×240	0438W	1×280	3×215	5×240	1.00
Apr 4	52369.24	0438E	...	2×215,	...	0438W	...	3×150,	...	0.58
			...	120	...		...	180	...	
Apr 12	52377.25	0438E	3×190	...	...	0438W	2×280	...	...	1.02
total		0438E	5050	7000	11280	0438W	5320	7510	10800	
Nov 18	52231.49	0749E	2×280	3×215	5×240	0749W	2×280	3×215	5×240	0.60
Nov 19	52232.47	0749E	2×280	3×215	5×240	0749W	2×280	3×215	4×240	0.68
Nov 23	52236.45	0749E	2×280	3×215	4×240	0749W	2×280	3×215	4×240	1.08
Dec 9	52252.44	0749E	2×280	3×215	4×240	0749W	2×280	3×215	3×240	0.96
Jan 9	52283.55	0749E	2×280	3×215	3×240	0749W	2×280	3×215	3×240	0.60
Jan 14	52288.54	0749E	2×280	3×215	5×240	0749W	2×280	3×215	5×240	0.66
Jan 15	52289.54	0749E	2×280	3×215	3×240	0749W	2×280	3×215	4×240	0.85
Feb 17	52323.43	0749E	2×280	3×215	5×220	0749W	2×280	3×215	5×220	0.88
Apr 4	52369.27	0749E	...	3×215	...	0749W	...	3×215	...	0.54
Apr 12	52377.27	0749E	2×280	...	...	0749W	2×280	...	...	0.75
Apr 13	52378.31	0749E	...	...	4×240	0749W	...	...	4×240	0.91
total		0749E	5040	5805	9020	0749W	5040	5805	8780	
Oct 16	52198.62	0848E	...	4×215	...	0848W	...	6×215	...	0.59

TABLE 3—*Continued*

date	MJD	field	R[1]	I[1]	Z[1]	field	R[1]	I[1]	Z[1]	FWHM[2]
Oct 22	52204.63	0848E	...	3×215	...	0848W	...	4×215	...	0.64
Nov 18	52231.60	0848E	2×280	5×215	5×240	0848W	2×280	5×215	5×240	0.57
Nov 19	52232.53	0848E	...	3×215	...	0848W	...	3×215	...	0.54
Nov 23	52236.54	0848E	2×280	3×215	4×240	0848W	2×280	3×215	4×240	1.04
Dec 9	52252.53	0848E	2×280	4×215	5×240	0848W	2×280	5×215	3×240	0.92
Jan 9	52283.53	0848E	2×280	3×215	4×240	0848W	2×280	3×215	4×240	0.72
Jan 14	52288.44	0848E	2×280	3×215	5×240	0848W	2×280	3×215	5×240	0.68
Jan 15	52289.51	0848E	2×280	3×215	3×240	0848W	2×280	3×215	3×240	0.61
Feb 17	52323.52	0848E	2×280	1×215	5×220	0848W	2×280	1×215	5×220	1.17
Apr 4	52369.32	0848E	...	3×215	3×240	0848W	...	3×215	5×200	0.68
		0848E	...	...	180,200					
Apr 12	52377.30	0848E	...	...	5×240	0848W	...	...	2×240,	0.71
						0848W	...	...	3×200	
Apr 13	52378.25	0848E	2×280	...	...	0848W	2×280	...	...	0.91
total		0848E	4480	7525	9640	0848W	4480	8385	8940	
Nov 19	52232.60	1052N	...	5×215	5×240	1052S	...	5×215	5×240	0.52
Nov 23	52236.62	1052N	2×280	3×215	3×240	1052S	2×280	3×215	3×240	0.98
Dec 9	52252.63	1052N	2×280	3×215	3×240	1052S	2×280	3×215	...	1.07
Jan 9	52283.64	1052N	2×280	3×215	2×240	1052S	2×280	3×215	2×240	0.73
Jan 14	52288.63	1052N	2×280	3×215	4×240	1052S	2×280	3×215	...	0.63
Jan 15	52289.56	1052N	2×280	2×215	3×240	1052S	2×280	2×215	3×240	0.60
Feb 17	52323.61	1052N	2×280	3×215	4×220	1052S	2×280	3×215	5×220	1.46
Apr 4	52369.39	1052N	...	...	9×200	1052S	...	...	8×200	0.72
Apr 12	52377.38	1052N	...	7×215	5×200	1052S	...	7×215	5×240	0.83
Apr 13	52378.35	1052N	2×280	...	9×240	1052S	2×280	...	8×240	0.94
total		1052N	3920	6235	10640	1052S	3920	6235	8940	

[1]All exposure times in seconds.

[2]arcseconds

TABLE 4
IFA DEEP SURVEY TYPE IA SUPERNOVAE

SN	R.A.[1](2000)	Dec.[2](2000)	$E(B-V)$[3]
2001fo	04:37:41.45	–01:29:33.1	0.037
2001fs	04:39:30.68	–01:28:21.9	0.030
2001hs	04:39:22.39	–01:32:51.4	0.032
2001hu	07:50:35.90	+09:58:14.2	0.021
2001hx	08:49:24.61	+44:02:22.4	0.031
2001hy	08:49:45.85	+44:15:31.8	0.032
2001iv	07:50:13.53	+10:17:10.4	0.022
2001iw	07:50:39.32	+10:20:19.1	0.022
2001ix	10:52:18.92	+57:07:29.6	0.009
2001iy	10:52:24.28	+57:16:36.1	0.007
2001jb	02:26:33.31	+00:25:35.0	0.032
2001jf	02:28:07.13	+00:26:45.1	0.028
2001jh	02:29:00.29	+00:20:44.2	0.026
2001jm	04:39:13.82	–01:23:18.2	0.033
2001jn	04:40:12.00	–01:17:45.9	0.031
2001jp	08:46:31.40	+44:03:56.6	0.030
2001kd	07:50:31.24	+10:21:07.3	0.023
2002P	02:29:05.71	+00:47:20.1	0.030
2002W	08:47:54.42	+44:13:42.9	0.029
2002X	08:48:30.54	+44:15:35.3	0.029
2002aa	07:48:45.28	+10:18:00.8	0.024
2002ab	07:48:55.70	+10:06:06.3	0.020
2002ad	10:50:12.19	+57:31:11.6	0.007

[1]hh:mm:ss

[2]dd:mm:ss

[3]Galactic Extinction (mag) from Schlegel, Finkbeiner, & Davis (1998)

TABLE 5
IFA DEEP SURVEY SNE IA SPECTROSCOPIC OBSERVATIONS

SN	MJD	Date[1]	Instrument	Integration (s)
2001fo	52204.0	Oct 21	Keck-II ESI	4400
2001fs	52205.0	Oct 22	Keck-II ESI	5400
2001hs	52232.9	Nov 18	Keck-II ESI	5400
2001hu	52233.0	Nov 18	Keck-II ESI	7800
2001hx	52233.0	Nov 18	Keck-II ESI	3000
2001hy	52232.1	Nov 17	Keck-II ESI	5500
2001iv	52257.4	Dec 13	VLT FORS1	2400
2001iw	52257.3	Dec 13	VLT FORS1	2400
2001ix	52267.1	Dec 22	Keck-I LRIS	3000
2001iy	52267.2	Dec 22	Keck-I LRIS	600
2001jb	52266.9	Dec 22	Keck-I LRIS	2400
2001jf	52266.8	Dec 22	Keck-I LRIS	3600
2001jh	52257.1	Dec 13	VLT FORS1	5400
2001jm	52257.2	Dec 13	VLT FORS1	5400
2001jm	52267.0	Dec 22	Keck-I LRIS	5400
2001jn	52585.0	Nov 06	Keck-II ESI	2700
2001jp	52267.1	Dec 22	Keck-I LRIS	1200
2001kd	52232.0	Nov 17	Keck-II ESI	7200
2002P	52291.8	Jan 16	Keck-I LRIS	3600
2002W	52292.1	Jan 16	Keck-I LRIS	3600
2002X	52292.0	Jan 16	Keck-I LRIS	2100
2002aa	52292.0	Jan 16	Keck-I LRIS	1200
2002ab	52292.0	Jan 16	Keck-I LRIS	900
2002ad	52292.1	Jan 16	Keck-I LRIS	1800

[1]2001 except for 2001jn, which was taken in 2002.

TABLE 6
SN SPECTROSCOPIC IDENTIFICATIONS

SN	Identification
2001fo	$z = 0.772 \pm 0.001$ from host [O II].
2001fs	$z = 0.874 \pm 0.010$ from correlating with SN Ia features.
2001hs	$z = 0.833 \pm 0.001$ from host [O II], [O III].
2001hu	$z = 0.882 \pm 0.001$ from host [O II]. Clear SN Ia features, strong correlation via SNID.
2001hx	$z = 0.799 \pm 0.001$ from host [O II].
2001hy	$z = 0.812 \pm 0.001$ from host [O II], possible Hβ.
2001iv	$z = 0.3965 \pm 0.0003$ from host Hα, Hβ, [O III]. Clear SN Ia features, strong correlation via SNID.
2001iw	$z = 0.3396 \pm 0.0001$ from host Hα, [O III]. Clear SN Ia features, strong correlation via SNID.
2001ix	$z = 0.711 \pm 0.010$ from correlating with SN Ia features.
2001iy	$z = 0.568 \pm 0.001$ from host [O II], Hβ. Clear SN Ia features, strong correlation via SNID.
2001jb	$z = 0.698 \pm 0.001$ from host [O II], [O III], and Hβ.
2001jf	$z = 0.815 \pm 0.001$ from host [O II], [O III].
2001jh	$z = 0.885 \pm 0.001$ from host [O II]. Clear SN Ia features, strong correlation via SNID.
2001jm	$z = 0.978 \pm 0.010$ from correlating with SN Ia features.
2001jn	$z = 0.645 \pm 0.001$ from host [O II].
2001jp	$z = 0.528 \pm 0.001$ from host [O II], [O III], Hβ. Clear SN Ia features, strong correlation via SNID.
2001kd	$z = 0.936 \pm 0.001$ from host [O II], 4000 Å break apparent.
2002P	$z = 0.719 \pm 0.001$ from host [O II]. Clear SN Ia features, strong correlation via SNID.
2002W	$z = 1.031 \pm 0.001$ from host [O II].
2002X	$z = 0.859 \pm 0.001$ from host [O II], [O III], Hβ.
2002aa	$z = 0.946 \pm 0.001$ from host [O II], 4000 Å break apparent.
2002ab	$z = 0.423 \pm 0.001$ from host [O II]. Clear SN Ia features, strong correlation via SNID.
2002ad	$z = 0.514 \pm 0.001$ from host [O II]. SN Ia somewhat diluted by host galaxy. Good correlation via SNID.

TABLE 7
SNID INFORMATION

SN	z_{em}[1]	epoch[2]	$z_{best,SNID}$[3]	r*lap[3]	t_{SNID}[3]	$z_{SNID}(z_{em})$[4]	r*lap(z_{em})[4]	$t_{SNID}(z_{em})$[4]
2001hu[5]	0.882	-2.9	0.869	5.8	-1.8			
2001iv[5]	0.3965	4.2	0.398	6.7	-0.5			
2001iw[5]	0.3396	5.1	0.342	9.3	2.4			
2001iy[5]	0.568	9.9	0.570	6.0	3.8			
2001jh[5]	0.885	3.5	0.901	7.3	-3.8			
2001jp[5]	0.528	-3.6	0.535	6.7	-5.7			
2002P[5]	0.719	-6.2	0.717	4.9	-2.8			
2002ab[5]	0.423	3.9	0.420	6.8	0.6			
2002ad[5]	0.514	15.2	0.765	5.3	1.9	0.510	3.0	11.8
2001fo[6]	0.772	-3.7	0.413	5.7	-7.6	0.774	3.9	14.5
2001hs[6]	0.833	-5.8	0.806	5.4	4.6	0.826	5.1	-3.1
2001hx[6]	0.799	-0.3	1.048	5.6	0.7	–	1.2	
2001hy[6]	0.812	-1.3	1.114	5.7	3.8	0.813	2.2	-0.9
2001jb[6]	0.698	8.5	0.218	5.6	-4.3	–	2.0	
2001jf[6]	0.815	0.2	–			0.827	2.8	3.0
2001jn[6]	0.645	N/A						
2001kd[6]	0.936	8.5	0.416	5.6	-6.1	0.938	2.3	11.0
2002W[6]	1.031	-4.1	1.053	4.5	-4.8			
2002X[6]	0.859	-4.0	0.863	3.5	-4.8			
2002aa[6]	0.946	9.5	0.499	4.9	11.1	0.944	2.9	-1.4
2001fs[7]	–	-0.9	0.874	7.7	-5.4			
2001ix[7]	–	-0.9	0.711	10.2	-1.0			
2001jm[7]	–	-0.6	0.978	4.1	-5.0			

[1]Host galaxy redshift as reported in Table 6.

[2]As determined by MLCS fits (see Section 5.1).

[3]Best fit parameters as determined by SNID. For SN 2001jf, there were no template matches with $r * lap > 3.0$. SN 2001jn was observed in 2002, long after the SN had faded from view.

[4]SNID parameters determined while constraining the redshift to the host-galaxy redshift as determined by emission lines.

[5]9 SNe for which there is unambiguous spectral confirmation by SNID as a SN Ia at the host-galaxy redshift.

[6]11 SNe for which there is substantial photometric evidence, but not unambiguous spectral confirmation, for identification as a SN Ia at the host galaxy redshift.

[7]3 SNe for which there is clear spectral identification by SNID as a SN Ia, but no host galaxy emission with which to confirm the redshift.

TABLE 8
SN 2001FO OBSERVATIONS

MJD	flux[1]	$\sigma(flux)^2$	epoch (rest)	K-correction(σ)
	I			$I \rightarrow B$
52164.57	0.000e+00	3.856e–02	-25.9	
52176.49	2.121e–02	1.845e–01	-19.2	
52191.50	2.818e+00	1.967e–01	-10.7	-1.128(0.040)
52204.59	7.106e+00	3.066e–01	-3.4	-1.160(0.040)
52225.39	5.854e+00	1.941e–01	8.4	-1.205(0.040)
52231.38	4.173e+00	2.044e–01	11.8	-1.235(0.040)
52232.35	4.051e+00	2.166e–01	12.3	-1.239(0.040)
52236.34	3.309e+00	2.796e–01	14.6	-1.256(0.040)
52252.35	1.309e+00	2.404e–01	23.6	-1.277(0.040)
52263.38	1.137e+00	3.753e–01	29.8	-1.269(0.040)
52283.39	5.289e–01	1.452e–01	41.1	
52288.23	8.426e–01	1.163e–01	43.8	
52289.38	3.406e–02	3.471e–01	44.5	
52323.35	2.828e–02	3.683e–01	63.7	
52369.25	-5.399e–01	3.747e–01	89.6	
	R			
52204.53	5.952e+00	1.696e–01	-3.4	
52231.34	2.502e+00	1.690e–01	11.7	
52232.34	2.243e+00	1.387e–01	12.3	
52236.38	1.885e+00	1.885e–01	14.6	
52252.38	6.506e–01	1.291e–01	23.6	
52283.36	2.139e–01	1.228e–01	41.1	
52288.25	2.302e–01	1.480e–01	43.9	
52289.27	2.151e–01	6.303e–02	44.4	
52323.37	-3.381e–01	3.923e–01	63.7	
52377.25	0.000e+00	2.167e–01	94.1	
	Z			$Z \rightarrow V$
52204.54	7.411e+00	3.003e–01	-3.4	-1.077(0.095)
52231.39	5.316e+00	2.354e–01	11.8	-1.003(0.095)
52232.40	5.593e+00	3.003e–01	12.3	-0.995(0.095)
52236.31	4.301e+00	3.583e–01	14.5	-0.961(0.095)
52252.31	2.334e+00	3.156e–01	23.6	-0.860(0.095)
52283.43	5.255e–01	3.412e–01	41.1	
52288.29	1.264e+00	2.423e–01	43.9	
52289.23	1.053e+00	3.583e–01	44.4	
52323.31	0.000e+00	5.357e–01	63.6	

[1]Magnitudes may be calculated from all flux values by $mag = -2.5\log(flux) + 25.0$

[2]Magnitude uncertainties may be calculated from all flux uncertainties by $\sigma(mag) = 2.5\log(1 + \sigma(flux)/flux)$.

TABLE 8
SN 2001FS OBSERVATIONS

MJD	flux[1]	$\sigma(flux)$[2]	epoch (rest)	K-correction(σ)
	I			$I \rightarrow B$
52164.57	-3.597e–01	1.022e–01	-22.4	
52176.49	-2.352e–03	1.819e–01	-16.1	
52191.50	1.617e+00	6.363e–02	-8.0	-1.250(0.044)
52198.59	-3.404e–01	7.314e–01	-4.3	
52204.58	2.377e+00	2.821e–01	-1.1	-1.243(0.044)
52225.39	1.193e+00	8.805e–02	10.0	-1.215(0.044)
52231.37	1.313e+00	1.819e–01	13.2	-1.176(0.044)
52232.36	8.781e–01	1.568e–01	13.7	-1.170(0.044)
52236.33	8.621e–01	2.667e–01	15.8	-1.152(0.044)
52252.34	-1.495e–01	3.284e–01	24.4	
52263.38	8.505e–02	4.936e–01	30.1	-1.167(0.044)
52283.38	2.207e–02	1.125e–01	40.7	
52288.22	-5.004e–01	4.222e–01	43.5	
52289.37	4.090e–01	3.381e–01	43.9	
52323.34	2.444e–01	5.360e–01	62.0	
52369.24	-2.851e–01	3.702e–01	86.8	
	R			
52204.52	1.167e+00	1.071e–01	-1.1	
52231.33	3.559e–01	1.188e–01	13.1	
52232.33	1.908e–01	9.968e–02	13.7	
52236.36	9.956e–03	8.357e–02	15.8	
52252.37	-5.247e–02	8.498e–02	24.3	
52283.35	8.205e–02	1.196e–01	40.7	
52288.25	3.223e–01	1.530e–02	43.3	
52289.26	3.356e–01	1.609e–01	43.9	
52323.37	-2.710e–02	2.328e–01	62.0	
52377.24	3.513e–02	2.408e–01	90.5	
	Z			$Z \rightarrow V$
52198.52	4.686e–01	1.572e+00	-4.3	
52204.56	3.623e+00	2.299e–01	-1.1	-1.089(0.165)
52231.43	2.169e+00	2.726e–01	13.2	-0.911(0.165)
52232.38	1.297e+00	3.261e–01	13.7	-0.889(0.165)
52236.29	1.923e+00	6.736e–01	15.8	-0.811(0.165)
52252.29	6.557e–01	7.537e–01	24.3	-0.707(0.165)
52283.41	1.960e–01	2.459e–01	40.8	
52288.27	3.029e–01	4.063e–01	43.3	
52289.21	-6.062e–02	1.818e–01	43.8	
52323.28	-1.001e+00	6.896e–01	61.9	

[1]Magnitudes may be calculated from all flux values by $mag = -2.5\log(flux) + 25.0$

[2]Magnitude uncertainties may be calculated from all flux uncertainties by $\sigma(mag) = 2.5\log(1 + \sigma(flux)/flux)$.

TABLE 8
SN 2001HS OBSERVATIONS

MJD	flux[1]	$\sigma(flux)$[2]	epoch (rest)	K-correction(σ)
	I			$I \rightarrow B$
52164.57	6.764e–01	1.343e–01	-43.0	
52176.49	5.318e–01	9.576e–02	-36.5	
52191.50	4.296e–01	2.397e–01	-28.4	
52198.59	-1.353e+00	1.204e+00	-24.5	
52204.58	2.408e–02	2.069e–01	-21.2	
52225.39	2.430e+00	1.144e–01	-9.9	-1.209(0.014)
52231.37	3.639e+00	1.215e–01	-6.6	-1.222(0.014)
52232.36	4.006e+00	8.998e–02	-6.1	-1.224(0.014)
52236.33	4.841e+00	4.049e–01	-3.9	-1.231(0.014)
52252.34	4.666e+00	2.487e–01	4.8	-1.249(0.014)
52263.38	2.639e+00	4.512e–01	10.8	-1.238(0.014)
52283.38	6.199e–01	1.086e–01	21.7	-1.216(0.014)
52288.22	3.249e–01	4.917e–01	24.4	-1.216(0.014)
52289.37	1.732e–01	3.246e–01	25.0	-1.216(0.014)
52323.34	8.514e–02	3.586e–01	43.5	
52369.24	-1.006e–01	2.866e–01	68.5	
	R			
52204.52	-1.021e–01	1.242e+00	-21.3	
52231.33	2.131e+00	3.849e+00	-6.6	
52232.33	2.491e+00	1.118e+00	-6.1	
52236.36	2.805e+00	1.509e+00	-3.9	
52252.37	1.340e+00	1.502e+00	4.8	
52283.35	-5.159e–02	3.741e+00	21.7	
52288.25	-1.042e–01	1.896e+00	24.4	
52289.26	1.498e–01	1.512e+00	24.9	
52323.37	4.859e–01	1.483e+00	43.5	
52377.24	-4.145e–01	1.486e+00	72.9	
	Z			$Z \rightarrow V$
52198.52	-2.945e+00	1.117e+00	-24.5	
52204.56	0.000e+00	3.421e–01	-21.2	
52231.43	3.614e+00	3.314e–01	-6.6	-1.150(0.126)
52232.38	3.683e+00	4.704e–01	-6.1	-1.158(0.126)
52236.29	4.752e+00	4.383e–01	-3.9	-1.153(0.126)
52252.29	4.490e+00	4.009e–01	4.8	-1.135(0.126)
52283.41	1.374e+00	7.003e–01	21.8	-0.842(0.126)
52288.27	9.729e–01	2.887e–01	24.4	-0.825(0.126)
52289.21	1.497e+00	4.063e–01	24.9	-0.823(0.126)
52323.28	-1.711e–01	8.553e–02	43.5	

[1]Magnitudes may be calculated from all flux values by $mag = -2.5\log(flux) + 25.0$

[2]Magnitude uncertainties may be calculated from all flux uncertainties by $\sigma(mag) = 2.5\log(1 + \sigma(flux)/flux)$.

TABLE 8
SN 2001HU OBSERVATIONS

MJD	flux[1]	$\sigma(flux)$[2]	epoch (rest)	K-correction(σ)
	I			$I \rightarrow B$
52195.57	0.000e+00	3.748e–01	-22.8	
52225.48	2.899e+00	2.171e–01	-6.9	-1.258(0.034)
52231.47	3.554e+00	3.374e–01	-3.7	-1.257(0.034)
52232.45	3.412e+00	3.539e–01	-3.2	-1.257(0.034)
52252.42	2.157e+00	4.514e–01	7.4	-1.254(0.034)
52262.50	1.275e+00	4.049e–01	12.8	-1.202(0.034)
52288.50	1.924e–01	4.122e–01	26.6	-1.168(0.034)
52289.54	5.746e–01	1.166e+00	27.1	-1.169(0.034)
52323.40	5.126e–01	1.231e+00	45.1	-1.178(0.034)
52369.26	2.891e–01	1.113e–01	69.5	-1.130(0.034)
	R			
52231.45	9.956e–01	6.533e–01	-3.7	
52232.43	8.732e–01	9.284e–01	-3.2	
52236.41	9.447e–01	2.676e+00	-1.1	
52252.40	1.509e–01	6.898e–01	7.4	
52283.57	-4.126e–02	1.385e+00	23.9	
52288.57	-1.766e–01	1.044e+00	26.6	
52289.57	-3.566e–01	1.918e+00	27.1	
52323.38	-7.287e–03	6.475e–01	45.1	
52377.26	-1.612e–01	1.033e+00	73.7	
	Z			$Z \rightarrow V$
52231.50	3.733e+00	3.632e–01	-3.7	-1.218(0.149)
52232.48	3.181e+00	2.991e–01	-3.2	-1.199(0.149)
52236.44	3.008e+00	8.636e–01	-1.1	-1.119(0.149)
52283.54	3.307e–01	1.328e–01	24.0	-0.813(0.149)
52288.52	4.430e–01	5.981e–01	26.6	-0.802(0.149)
52289.49	3.846e–01	2.568e–01	27.1	-0.801(0.149)
52323.44	2.898e–01	8.257e–01	45.1	-0.790(0.149)
52378.30	-3.973e–01	4.887e–01	74.3	

[1]Magnitudes may be calculated from all flux values by $mag = -2.5\log(flux) + 25.0$

[2]Magnitude uncertainties may be calculated from all flux uncertainties by $\sigma(mag) = 2.5\log(1 + \sigma(flux)/flux)$.

TABLE 8
SN 2001HX OBSERVATIONS

MJD	flux[1]	$\sigma(flux)$[2]	epoch (rest)	K-correction(σ)
	I			$I \rightarrow B$
52191.56	-2.000e–01	4.762e–01	-23.3	
52198.61	-8.001e–01	3.593e–01	-19.4	
52204.61	2.814e–01	1.575e–01	-16.1	-1.109(0.031)
52225.56	3.053e+00	6.549e–01	-4.4	-1.205(0.031)
52231.63	3.689e+00	2.443e–01	-1.1	-1.197(0.031)
52232.52	3.815e+00	1.257e–01	-0.6	-1.196(0.031)
52236.50	3.418e+00	5.841e–02	1.6	-1.199(0.031)
52252.53	2.198e+00	2.425e–01	10.6	-1.236(0.031)
52263.51	1.441e+00	3.576e–01	16.7	-1.242(0.031)
52283.49	3.770e–01	3.646e–01	27.8	-1.250(0.031)
52288.47	3.823e–01	2.832e–02	30.5	-1.252(0.031)
52289.41	3.894e–02	8.674e–02	31.1	-1.252(0.031)
52323.55	-5.098e–01	1.427e+00	50.0	
52369.29	0.000e+00	1.310e–01	75.5	
	R			
52231.59	1.308e+00	4.589e–02	-1.1	
52236.57	1.305e+00	1.579e–01	1.7	
52252.57	4.298e–01	1.692e–01	10.6	
52283.59	-1.617e–01	8.961e–02	27.8	
52288.40	1.007e–01	1.467e–01	30.5	
52289.59	-3.193e–02	3.367e–02	31.1	
52323.53	-8.141e–01	2.985e–01	50.0	
52378.24	1.877e–01	5.963e–02	80.4	
	Z			$Z \rightarrow V$
52231.54	3.562e+00	3.176e–01	-1.1	-1.061(0.112)
52236.55	3.644e+00	4.737e–01	1.7	-1.052(0.112)
52252.48	2.044e+00	4.597e–01	10.5	-1.015(0.112)
52283.45	4.737e–01	1.351e–01	27.7	-0.909(0.112)
52288.43	4.068e–01	2.480e–01	30.5	-0.805(0.112)
52289.44	8.526e–01	3.943e–01	31.1	-0.805(0.112)
52323.48	-2.926e–02	4.792e–01	50.0	
52369.32	-5.141e–01	5.085e–01	75.4	
52377.29	0.000e+00	2.926e–01	79.9	

[1]Magnitudes may be calculated from all flux values by $mag = -2.5\log(flux) + 25.0$

[2]Magnitude uncertainties may be calculated from all flux uncertainties by $\sigma(mag) = 2.5\log(1 + \sigma(flux)/flux)$.

TABLE 8
SN 2001HY OBSERVATIONS

MJD	flux[1]	$\sigma(flux)$[2]	epoch (rest)	K-correction(σ)
	I			$I \rightarrow B$
52191.56	-5.605e–02	3.965e–01	-23.7	
52198.61	-2.720e–01	5.771e–01	-19.8	
52204.61	8.839e–01	2.160e–01	-16.5	-1.166(0.023)
52225.56	2.976e+00	2.584e–01	-5.0	-1.205(0.023)
52231.63	3.235e+00	1.965e–01	-1.6	-1.216(0.023)
52232.52	3.537e+00	9.913e–02	-1.1	-1.217(0.023)
52236.50	3.220e+00	1.682e–01	1.1	-1.222(0.023)
52252.53	1.597e+00	8.320e–02	9.9	-1.237(0.023)
52263.51	1.103e+00	4.779e–01	16.0	-1.241(0.023)
52283.49	7.493e–02	2.567e–01	27.0	
52288.47	4.661e–01	3.045e–01	29.8	-1.235(0.023)
52289.41	-8.261e–02	4.815e–01	30.2	
52323.55	-1.947e+00	1.498e+00	49.1	
52369.29	4.484e–02	3.381e–01	74.4	
	R			
52231.59	1.415e+00	8.844e–02	-1.6	
52236.57	1.299e+00	6.482e–02	1.1	
52252.57	4.908e–01	1.224e–01	10.0	
52283.59	1.191e–01	9.028e–02	27.1	
52288.40	8.557e–03	7.236e–02	29.7	
52289.59	2.159e–01	4.623e–02	30.4	
52323.53	-1.156e–01	2.698e–01	49.1	
52378.24	-3.206e–04	8.241e–02	79.3	
	Z			$Z \rightarrow V$
52231.54	2.886e+00	1.881e–01	-1.7	-1.067(0.123)
52236.55	3.205e+00	6.200e–01	1.1	-1.048(0.123)
52252.48	1.015e+00	7.899e–01	9.9	-1.018(0.123)
52283.45	5.233e–02	2.689e–01	27.0	-0.780(0.123)
52288.43	1.916e–01	4.040e–01	29.7	-0.801(0.123)
52289.44	1.359e–01	3.915e–01	30.3	-0.803(0.123)
52323.48	2.279e–01	2.452e–01	49.1	
52369.32	1.192e–02	4.152e–01	74.3	
52377.29	-3.949e–01	3.720e–01	78.8	

[1]Magnitudes may be calculated from all flux values by $mag = -2.5\log(flux) + 25.0$

[2]Magnitude uncertainties may be calculated from all flux uncertainties by $\sigma(mag) = 2.5\log(1 + \sigma(flux)/flux)$.

TABLE 8
SN 2001IV OBSERVATIONS

MJD	flux[1]	$\sigma(flux)^2$	epoch (rest)	K-correction(σ)
	I			$I \rightarrow V$
52195.57	0.000e+00	2.225e–01	-40.1	
52225.48	-9.193e–01	4.660e–01	-18.7	
52231.48	8.874e–01	2.043e–01	-14.4	-0.756(0.052)
52232.46	1.969e+00	1.569e–01	-13.7	-0.757(0.052)
52236.49	6.649e+00	1.751e–01	-10.8	-0.768(0.052)
52252.43	2.106e+01	3.438e–01	0.6	-0.820(0.052)
52262.50	1.818e+01	2.727e–01	7.8	-0.767(0.052)
52283.53	8.977e+00	1.715e–01	22.9	-0.885(0.052)
52288.51	7.955e+00	1.222e–01	26.5	-0.900(0.052)
52289.56	7.273e+00	2.873e–01	27.2	-0.903(0.052)
52323.41	2.349e+00	2.353e–01	51.4	
52369.27	4.514e–01	1.678e–01	84.3	
	R			$R \rightarrow B$
52231.46	1.013e+00	1.161e–01	-14.4	-0.656(0.066)
52232.44	1.592e+00	2.185e–01	-13.7	-0.655(0.066)
52236.42	5.613e+00	1.265e–01	-10.8	-0.647(0.066)
52252.41	1.733e+01	2.325e–01	0.6	-0.660(0.066)
52283.58	3.902e+00	1.749e–02	22.9	-0.854(0.066)
52288.58	2.490e+00	9.203e–02	26.5	-0.855(0.066)
52289.58	2.085e+00	1.782e–01	27.2	-0.855(0.066)
52323.38	5.524e–01	8.290e–02	51.4	
52377.27	0.000e+00	4.107e–02	90.0	
	Z			
52231.52	2.198e+00	3.399e–01	-14.4	
52232.50	1.606e+00	3.997e–01	-13.7	
52236.45	8.811e+00	3.924e–01	-10.8	
52252.46	2.072e+01	5.967e–01	0.6	
52283.56	1.060e+01	3.953e–01	22.9	
52288.54	9.535e+00	2.378e–01	26.5	
52289.50	9.748e+00	5.047e–01	27.2	
52323.46	2.375e+00	3.209e–01	51.5	
52378.31	0.000e+00	4.479e–01	90.8	

[1]Magnitudes may be calculated from all flux values by $mag = -2.5\log(flux) + 25.0$

[2]Magnitude uncertainties may be calculated from all flux uncertainties by $\sigma(mag) = 2.5\log(1 + \sigma(flux)/flux)$.

TABLE 8
SN 2001IW OBSERVATIONS

MJD	flux[1]	$\sigma(flux)$[2]	epoch (rest)	K-correction(σ)
	I			$I \rightarrow V$
52195.57	-2.660e–02	1.514e–01	-41.0	
52225.48	2.826e–01	4.934e–01	-18.7	-0.777(0.094)
52231.47	4.437e+00	2.353e–01	-14.2	-0.772(0.094)
52232.45	5.048e+00	3.475e–01	-13.5	-0.772(0.094)
52236.48	1.202e+01	1.979e–01	-10.5	-0.773(0.094)
52252.42	2.971e+01	3.037e–01	1.4	-0.804(0.094)
52262.50	1.815e+01	2.289e–01	9.0	-0.649(0.094)
52283.52	1.151e+01	1.268e–01	24.7	-0.871(0.094)
52288.50	9.747e+00	2.125e–01	28.4	-0.907(0.094)
52289.54	9.482e+00	2.462e–02	29.2	-0.914(0.094)
52323.40	3.229e+00	3.739e–02	54.4	
52369.26	1.653e+00	3.502e–01	88.7	
	R			$R \rightarrow B$
52231.45	2.233e+00	1.341e–01	-14.2	-0.626(0.101)
52232.43	3.416e+00	3.042e–02	-13.5	-0.624(0.101)
52236.41	8.878e+00	5.319e–01	-10.5	-0.611(0.101)
52252.40	2.216e+01	2.905e–01	1.4	-0.600(0.101)
52283.57	3.892e+00	5.273e–02	24.7	-0.935(0.101)
52288.57	2.341e+00	9.101e–02	28.4	-0.946(0.101)
52289.57	2.463e+00	1.255e–01	29.2	-0.947(0.101)
52323.38	4.421e–01	1.899e–01	54.4	
52377.26	0.000e+00	2.500e–01	94.6	
	Z			
52231.50	3.673e+00	4.756e–01	-14.1	
52232.48	5.176e+00	3.268e–01	13.4	
52236.44	1.249e+01	4.945e–01	10.5	
52252.45	2.642e+01	3.895e–01	1.5	
52283.54	1.278e+01	2.888e–01	24.7	
52288.52	1.122e+01	1.196e–01	28.4	
52289.49	9.647e+00	1.969e–01	29.1	
52323.44	1.778e+00	4.376e–01	54.5	
52378.30	0.000e+00	5.179e–01	95.4	

[1]Magnitudes may be calculated from all flux values by $mag = -2.5\log(flux) + 25.0$

[2]Magnitude uncertainties may be calculated from all flux uncertainties by $\sigma(mag) = 2.5\log(1 + \sigma(flux)/flux)$.

TABLE 8
SN 2001IX OBSERVATIONS

MJD	flux[1]	$\sigma(flux)$[2]	epoch (rest)	K-correction(σ)
	I			$I \rightarrow B$
52232.56	0.000e+00	2.125e–01	-21.0	
52236.65	-4.059e–01	5.740e–01	-18.6	
52252.62	3.895e+00	3.580e–01	-9.3	-1.119(0.068)
52263.57	6.942e+00	3.101e–01	-2.9	-1.113(0.068)
52283.64	5.446e+00	3.597e–01	8.8	-1.141(0.068)
52288.63	4.363e+00	9.581e–02	11.7	-1.172(0.068)
52289.66	4.406e+00	2.265e–01	12.3	-1.179(0.068)
52323.57	1.147e+00	5.278e–01	32.0	-1.276(0.068)
52377.41	2.778e–01	8.710e–02	63.4	
	R			
52236.59	0.000e+00	1.698e–01	-18.7	
52252.60	3.233e+00	1.939e–01	-9.3	
52283.62	3.203e+00	5.682e–02	8.8	
52288.60	2.322e+00	1.436e–01	11.7	
52289.64	2.218e+00	7.661e–02	12.3	
52323.60	5.082e–01	3.850e–01	32.1	
52378.28	3.260e–01	8.896e–02	63.9	
	Z			$Z \rightarrow V$
52232.61	3.828e–01	4.295e–01	-21.0	
52236.62	-1.934e+00	1.035e+00	-18.7	
52283.67	5.997e+00	6.007e–01	8.8	-1.104(0.063)
52288.66	6.253e+00	4.961e–01	11.7	-1.093(0.063)
52289.48	6.455e+00	9.034e–02	12.2	-1.090(0.063)
52323.63	2.798e+00	6.007e–01	32.1	-0.910(0.063)
52369.38	1.671e–02	1.716e+00	58.8	
52377.35	-3.066e–01	8.289e–01	63.4	
52378.35	3.971e–01	9.494e–01	64.0	

[1]Magnitudes may be calculated from all flux values by $mag = -2.5\log(flux) + 25.0$

[2]Magnitude uncertainties may be calculated from all flux uncertainties by $\sigma(mag) = 2.5\log(1 + \sigma(flux)/flux)$.

TABLE 8
SN 2001IY OBSERVATIONS

MJD	flux[1]	$\sigma(flux)$[2]	epoch (rest)	K-correction(σ)
	I			$I \rightarrow V$
52232.56	1.446e+00	2.090e–02	-12.1	-0.850(0.075)
52236.65	4.244e+00	1.403e+00	-9.5	-0.879(0.075)
52252.62	1.085e+01	4.390e–01	0.7	-0.858(0.075)
52263.57	9.823e+00	3.911e–01	7.7	-0.894(0.075)
52283.64	4.604e+00	5.731e–01	20.5	-0.785(0.075)
52288.63	3.529e+00	3.423e–01	23.6	-0.765(0.075)
52289.66	3.781e+00	5.069e–01	24.3	-0.762(0.075)
52323.57	6.602e–01	1.124e–01	45.9	
52377.41	2.475e–16	7.334e–01	80.2	
	R			$R \rightarrow B$
52236.59	5.481e+00	1.347e–01	-9.5	-0.645(0.055)
52252.60	1.090e+01	1.896e–01	0.7	-0.624(0.055)
52283.62	1.786e+00	9.683e–02	20.4	-0.569(0.055)
52288.60	1.447e+00	1.579e–01	23.6	-0.569(0.055)
52289.64	1.270e+00	6.555e–02	24.3	-0.569(0.055)
52323.60	1.964e–02	3.767e–01	45.9	
52378.28	-1.219e–03	9.385e–02	80.8	
	Z			
52232.61	1.786e+00	3.677e–01	-12.1	
52236.62	5.113e+00	5.769e–01	-9.5	
52283.67	4.769e+00	4.596e–01	20.5	
52288.66	5.275e+00	1.712e–01	23.7	
52289.48	4.796e+00	2.298e–01	24.2	
52323.63	4.110e+00	9.018e–01	46.0	
52369.38	-2.252e–16	1.377e+00	75.1	
52377.35	-1.743e–01	1.712e–01	80.2	
52378.35	7.100e–01	3.265e–01	80.9	

[1]Magnitudes may be calculated from all flux values by $mag = -2.5\log(flux) + 25.0$

[2]Magnitude uncertainties may be calculated from all flux uncertainties by $\sigma(mag) = 2.5\log(1 + \sigma(flux)/flux)$.

TABLE 8
SN 2001JB OBSERVATIONS

MJD	flux[1]	$\sigma(flux)$[2]	epoch (rest)	K-correction(σ)
	I			$I \rightarrow V$
52163.54	3.590e–01	9.767e–01	-52.4	
52174.56	-8.964e–02	2.353e–01	-45.9	
52191.43	2.275e–01	9.035e–01	-36.0	
52198.45	-3.927e–02	5.627e–01	-31.9	
52204.46	1.756e–01	4.148e–01	-28.3	
52225.31	3.417e–01	4.581e–01	-16.0	-0.819(0.150)
52231.24	9.052e–01	3.463e–01	-12.5	-0.854(0.150)
52232.26	1.180e+00	4.974e–01	-11.9	-0.867(0.150)
52236.24	2.134e+00	4.305e–01	-9.6	-0.932(0.150)
52252.23	4.962e+00	4.533e–01	-0.2	-0.950(0.150)
52263.23	3.705e+00	4.541e–01	6.3	-0.968(0.150)
52283.28	1.987e+00	5.210e–01	18.1	-0.587(0.150)
52288.36	1.578e+00	4.793e–01	21.1	-0.528(0.150)
52289.36	1.478e+00	1.310e+00	21.7	-0.519(0.150)
52323.23	1.351e+00	2.193e+00	41.6	
	R			$R \rightarrow B$
52204.51	7.520e–02	1.192e–01	-28.3	
52231.27	2.252e–01	1.067e–01	-12.5	-0.374(0.148)
52232.23	9.051e–02	2.626e–01	-12.0	-0.396(0.148)
52236.21	4.895e–01	1.985e–01	-9.6	-0.508(0.148)
52252.21	3.398e+00	2.426e–01	-0.2	-0.488(0.148)
52283.34	3.524e–01	1.434e–01	18.1	-0.249(0.148)
52288.39	2.756e–01	1.441e–01	21.1	-0.243(0.148)
52289.29	-5.715e–02	2.087e–01	21.7	
	Z			
52198.46	-3.272e+00	2.664e+00	-31.9	
52204.44	0.000e+00	1.649e–01	-28.3	
52231.31	1.108e+00	8.707e–01	-12.5	
52232.30	1.149e+00	7.471e–01	-11.9	
52236.27	1.005e+00	5.771e–01	-9.6	
52252.27	5.235e+00	9.583e–01	-0.2	
52283.31	2.246e+00	7.213e–01	18.1	
52288.33	2.313e+00	6.595e–01	21.1	
52289.32	1.669e+00	1.118e+00	21.7	
52323.26	-1.767e+00	3.091e+00	41.6	

[1]Magnitudes may be calculated from all flux values by $mag = -2.5\log(flux) + 25.0$

[2]Magnitude uncertainties may be calculated from all flux uncertainties by $\sigma(mag) = 2.5\log(1 + \sigma(flux)/flux)$.

TABLE 8
SN 2001JF OBSERVATIONS

MJD	flux[1]	$\sigma(flux)$[2]	epoch (rest)	K-correction(σ)
	I			$I \rightarrow B$
52163.54	-1.126e–01	6.847e–02	-56.7	
52174.56	3.321e–01	8.107e–02	-50.6	
52191.43	-2.826e–01	2.078e–01	-41.3	
52198.45	-2.267e–01	3.849e–01	-37.5	
52204.46	-2.440e–01	1.220e–01	-34.2	
52225.31	-1.891e–02	1.850e–01	-22.6	
52231.24	-1.700e–01	3.864e–01	-19.4	
52232.26	-1.496e–01	2.888e–01	-18.8	
52236.24	8.262e–02	4.801e–01	-16.7	-1.168(0.023)
52252.23	2.543e+00	3.069e–01	-7.8	-1.194(0.023)
52263.23	4.113e+00	4.085e–01	-1.8	-1.215(0.023)
52283.28	2.627e+00	6.249e–01	9.3	-1.232(0.023)
52288.36	2.198e+00	9.523e–02	12.1	-1.233(0.023)
52289.36	2.574e+00	3.432e–01	12.6	-1.232(0.023)
52323.23	3.304e–02	4.124e–01	31.3	-1.230(0.023)
	R			
52204.51	6.669e–02	1.234e–01	-34.1	
52231.27	4.500e–02	1.516e–01	-19.4	
52232.23	-2.432e–02	6.617e–02	-18.8	
52236.21	9.153e–02	1.807e–01	-16.7	
52252.21	1.598e+00	3.453e–01	-7.9	
52283.34	9.666e–01	1.021e–01	9.3	
52288.39	6.606e–01	1.981e–01	12.1	
52289.29	9.514e–01	1.407e–01	12.6	
	Z			$Z \rightarrow V$
52198.46	5.307e–01	1.190e+00	-37.5	
52204.44	-4.173e–01	6.698e–02	-34.1	
52231.31	-2.628e–01	4.637e–02	-19.3	
52232.30	-5.204e–01	1.752e–01	-18.8	
52236.27	1.597e–01	5.977e–01	-16.6	-0.940(0.119)
52252.27	2.664e+00	7.368e–01	-7.8	-1.110(0.119)
52283.31	2.545e+00	4.225e–01	9.3	-1.121(0.119)
52288.33	2.355e+00	2.215e–01	12.0	-1.088(0.119)
52289.32	2.988e+00	6.028e–01	12.6	-1.080(0.119)
52323.26	-9.152e–17	9.017e–01	31.3	

[1]Magnitudes may be calculated from all flux values by $mag = -2.5\log(flux) + 25.0$

[2]Magnitude uncertainties may be calculated from all flux uncertainties by $\sigma(mag) = 2.5\log(1 + \sigma(flux)/flux)$.

TABLE 8
SN 2001JH OBSERVATIONS

MJD	flux[1]	$\sigma(flux)$[2]	epoch (rest)	K-correction(σ)
	I			$I \rightarrow B$
52163.54	7.903e–02	2.723e–01	-46.1	
52174.56	-9.379e–02	2.016e–01	-40.3	
52191.43	2.100e–01	2.422e–01	-31.3	
52198.43	1.713e–01	2.154e–01	-27.6	
52204.48	6.856e–02	2.350e–01	-24.4	
52225.31	9.170e–01	2.232e–01	-13.4	-1.256(0.035)
52231.23	2.506e+00	3.339e–01	-10.2	-1.258(0.035)
52232.25	2.899e+00	6.546e–02	-9.7	-1.258(0.035)
52236.23	4.217e+00	2.363e–01	-7.6	-1.260(0.035)
52252.22	6.381e+00	2.952e–01	0.9	-1.262(0.035)
52263.23	4.572e+00	3.319e–01	6.8	-1.265(0.035)
52283.27	2.084e+00	2.664e–01	17.4	-1.203(0.035)
52288.21	1.402e+00	8.445e–02	20.0	-1.195(0.035)
52289.35	6.034e–01	6.494e–01	20.6	-1.193(0.035)
52323.22	7.874e–01	8.052e–01	38.6	-1.180(0.035)
	R			
52204.49	0.000e+00	2.543e–02	-24.4	
52231.26	1.772e+00	2.115e–01	-10.2	
52232.21	2.015e+00	1.213e–01	-9.7	
52236.20	2.756e+00	2.925e–01	-7.6	
52252.20	3.654e+00	3.193e–01	0.9	
52283.33	6.177e–01	1.088e–01	17.4	
52288.38	3.087e–01	4.427e–02	20.1	
52289.28	1.809e–01	1.531e–01	20.6	
	Z			$Z \rightarrow V$
52198.50	-4.122e–01	2.432e+00	-27.6	
52204.42	0.000e+00	7.213e–01	-24.4	
52231.29	2.169e+00	6.801e–01	-10.2	-1.113(0.146)
52232.28	3.308e+00	1.164e+00	-9.7	-1.132(0.146)
52236.25	3.746e+00	5.307e–01	-7.6	-1.201(0.146)
52252.25	6.172e+00	1.237e–01	0.9	-1.189(0.146)
52283.29	2.705e+00	5.358e–01	17.4	-1.069(0.146)
52288.30	2.968e+00	4.276e–01	20.1	-1.007(0.146)
52289.31	1.571e+00	5.049e–01	20.6	-0.996(0.146)
52323.25	2.303e+00	1.097e+00	38.6	-0.786(0.146)

[1]Magnitudes may be calculated from all flux values by $mag = -2.5\log(flux) + 25.0$

[2]Magnitude uncertainties may be calculated from all flux uncertainties by $\sigma(mag) = 2.5\log(1 + \sigma(flux)/flux)$.

TABLE 8
SN 2001JM OBSERVATIONS

MJD	flux[1]	$\sigma(flux)$[2]	epoch (rest)	K-correction(σ)
	I			$I \rightarrow B$
52164.57	2.282e–02	2.166e–01	-48.3	
52176.49	-2.795e–02	2.397e–01	-42.1	
52191.50	-3.037e–01	1.362e–01	-34.4	
52198.59	4.888e–01	5.624e–01	-30.8	
52204.58	2.465e–01	2.108e–01	-27.7	
52225.39	-2.066e–01	1.620e–01	-17.0	
52231.37	5.518e–01	2.776e–01	-13.9	-1.243(0.073)
52232.36	6.835e–01	1.755e–01	-13.4	-1.244(0.073)
52236.33	1.609e+00	2.988e–01	-11.4	-1.247(0.073)
52252.34	4.943e+00	3.098e–01	-3.1	-1.220(0.073)
52263.38	3.952e+00	2.892e–01	2.5	-1.193(0.073)
52283.38	1.948e+00	2.539e–01	12.8	-1.109(0.073)
52288.22	1.529e+00	1.832e–01	15.3	-1.079(0.073)
52289.37	1.257e+00	2.828e–01	15.9	-1.074(0.073)
52323.34	-3.538e–01	4.955e–01	33.4	
52369.24	3.107e–01	4.570e–01	57.0	
	R			
52204.52	-4.320e–02	9.263e–02	-27.7	
52231.33	1.943e–02	6.484e–02	-13.9	
52232.33	-1.254e–01	1.885e–01	-13.4	
52236.36	3.632e–01	6.786e–02	-11.3	
52252.37	1.776e+00	1.136e–01	-3.1	
52283.35	5.372e–01	1.152e–01	12.8	
52288.25	5.170e–01	9.283e–02	15.3	
52289.26	3.197e–01	1.263e–01	15.9	
52323.37	7.440e–02	4.237e–01	33.4	
52377.24	1.606e–01	2.177e–01	61.1	
	Z			$Z \rightarrow V$
52198.52	-2.336e+00	1.646e+00	-30.1	
52204.56	0.000e+00	4.170e–01	-27.7	
52231.43	4.971e–01	4.704e–01	-13.9	-1.090(0.175)
52232.38	7.003e–01	1.497e–01	-13.4	-1.098(0.175)
52236.29	1.181e+00	2.138e–01	-11.4	-1.145(0.175)
52252.29	4.816e+00	5.346e–02	-3.2	-1.246(0.175)
52283.41	2.357e+00	8.286e–01	12.8	-1.015(0.175)
52288.27	1.598e+00	2.352e–01	15.3	-0.911(0.175)
52289.21	2.101e+00	2.994e–01	15.8	-0.893(0.175)
52323.28	3.849e–01	3.261e–01	33.3	-0.658(0.175)

[1]Magnitudes may be calculated from all flux values by $mag = -2.5\log(flux) + 25.0$

[2]Magnitude uncertainties may be calculated from all flux uncertainties by $\sigma(mag) = 2.5\log(1 + \sigma(flux)/flux)$.

TABLE 8
SN 2001JN OBSERVATIONS

MJD	flux[1]	$\sigma(flux)$[2]	epoch (rest)	K-correction(σ)
	I			$I \rightarrow V$
52198.59	-1.426e+00	7.186e–01	-40.0	
52204.58	-6.884e–03	1.153e–01	-36.4	
52231.37	-1.488e–01	3.549e–02	-20.1	
52232.36	4.278e–01	8.872e–02	-19.5	
52236.33	8.714e–01	3.282e–01	-17.0	-0.790(0.136)
52252.34	3.196e+00	2.839e–01	-7.3	-0.929(0.136)
52283.38	2.894e+00	1.419e–01	11.6	-0.797(0.136)
52288.22	2.211e+00	2.750e–01	14.5	-0.691(0.136)
52289.37	1.883e+00	4.702e–01	15.2	-0.668(0.136)
52323.34	1.617e–01	5.589e–01	35.9	-0.539(0.136)
52369.24	1.705e–01	2.839e–01	63.8	
	R			$R \rightarrow B$
52204.52	0.000e+00	1.637e–01	-36.4	
52231.33	2.296e–02	1.140e–01	-20.1	
52232.33	2.557e–02	1.267e–01	-19.5	
52236.36	3.105e–01	1.335e–01	-17.0	-0.410(0.113)
52252.37	2.163e+00	2.900e–02	-7.3	-0.619(0.113)
52283.35	9.124e–01	2.165e–01	11.5	-0.395(0.113)
52288.25	6.770e–01	1.583e–01	14.5	-0.357(0.113)
52289.26	9.229e–01	6.243e–02	15.1	-0.351(0.113)
52323.37	-3.524e–01	3.272e–01	35.9	
52377.24	-2.267e–01	1.702e–01	68.6	
	Z			
52198.52	-6.155e+00	1.427e+00	-40.0	
52204.56	3.507e–02	2.459e–01	-36.4	
52231.43	1.903e–02	4.383e–01	-20.0	
52232.38	4.467e–01	4.116e–01	-19.4	
52236.29	-5.046e–02	2.726e–01	-17.0	
52252.29	3.740e+00	3.207e–01	-7.3	
52283.41	3.066e+00	2.619e–01	11.6	
52288.27	3.841e+00	1.016e–01	14.5	
52289.21	3.499e+00	3.100e–01	15.1	
52323.28	1.815e+00	7.056e–01	35.8	

[1]Magnitudes may be calculated from all flux values by $mag = -2.5\log(flux) + 25.0$

[2]Magnitude uncertainties may be calculated from all flux uncertainties by $\sigma(mag) = 2.5\log(1 + \sigma(flux)/flux)$.

TABLE 8
SN 2001JP OBSERVATIONS

MJD	flux[1]	$\sigma(flux)$[2]	epoch (rest)	K-correction(σ)
	I			$I \rightarrow V$
52198.62	3.052e–02	4.703e–01	-48.4	
52204.63	-3.076e–03	1.493e–01	-44.5	
52231.61	4.038e–01	2.613e–01	-26.8	
52232.54	4.150e–01	9.331e–02	-26.2	
52236.51	-5.368e–01	3.658e–01	-23.6	
52252.54	3.125e+00	1.493e–01	-13.1	-0.853(0.048)
52283.50	1.110e+01	1.418e–01	7.1	-0.877(0.048)
52288.48	9.496e+00	9.705e–02	10.4	-0.882(0.048)
52289.42	9.366e+00	6.719e–02	11.0	-0.883(0.048)
52323.56	2.158e+00	8.547e–01	33.3	-0.806(0.048)
52369.31	1.161e+00	5.972e–02	63.3	
	R			$R \rightarrow B$
52231.60	3.904e–03	5.243e–02	-26.8	
52236.57	-1.103e–01	2.787e–01	-17.0	
52252.58	2.091e+00	4.233e–01	-13.1	-0.678(0.029)
52283.60	8.734e+00	1.002e–01	7.2	-0.657(0.029)
52288.41	6.908e+00	6.348e–02	10.3	-0.662(0.029)
52289.60	5.931e+00	1.439e–01	11.1	-0.663(0.029)
52323.54	2.193e+00	5.593e–01	33.3	-0.650(0.029)
52378.25	7.147e–01	7.956e–02	69.1	
	Z			
52231.57	0.000e+00	9.571e–01	-26.9	
52236.53	-3.344e–02	1.078e+00	-23.6	
52252.50	1.434e+00	1.980e+00	-13.2	
52283.47	1.283e+01	4.988e–01	7.1	
52288.44	9.380e+00	8.289e–01	10.4	
52289.61	8.769e+00	7.105e–01	11.1	
52323.50	4.124e+00	8.665e–01	33.3	
52369.34	-5.426e+00	3.213e+00	63.3	
52377.31	1.209e+00	5.921e–01	68.5	

[1]Magnitudes may be calculated from all flux values by $mag = -2.5\log(flux) + 25.0$

[2]Magnitude uncertainties may be calculated from all flux uncertainties by $\sigma(mag) = 2.5\log(1 + \sigma(flux)/flux)$.

TABLE 8
SN 2001KD OBSERVATIONS

MJD	flux[1]	$\sigma(flux)$[2]	epoch (rest)	K-correction(σ)
	I			$I \rightarrow B$
52195.57	-2.751e–02	2.043e–01	-10.3	
52225.48	3.423e+00	3.110e–01	5.2	-1.208(0.063)
52231.47	2.759e+00	1.632e–01	8.2	-1.186(0.063)
52232.45	2.799e+00	1.870e–01	8.8	-1.181(0.063)
52236.48	2.211e+00	3.785e–01	10.8	-1.155(0.063)
52252.42	7.468e–01	2.645e–01	19.1	-1.077(0.063)
52262.50	4.887e–01	2.043e–01	24.3	-1.071(0.063)
52283.52	2.771e–01	2.572e–01	35.1	-1.077(0.063)
52288.50	3.546e–01	2.380e–01	37.7	-1.073(0.063)
52289.54	2.812e–02	2.554e–01	38.2	-1.072(0.063)
52323.40	1.991e–02	2.955e–01	55.7	
52369.26	3.163e–01	2.481e–01	79.4	
	R			
52231.45	6.428e–01	4.791e–02	8.2	
52232.43	4.937e–01	3.133e–01	8.7	
52236.41	1.750e–01	5.250e–01	10.8	
52252.40	2.681e–01	3.113e–01	19.1	
52283.57	-4.552e–02	2.003e–01	35.2	
52288.57	2.308e–01	1.998e–01	37.7	
52289.57	9.645e–02	2.358e–02	38.3	
52323.38	-5.439e–02	1.336e–01	55.7	
52377.26	6.476e–02	1.351e–01	83.6	
	Z			$Z \rightarrow V$
52231.50	3.837e+00	5.368e–01	8.3	-1.207(0.158)
52232.48	3.223e+00	5.047e–01	8.8	-1.192(0.158)
52236.44	3.701e+00	7.323e–01	10.8	-1.120(0.158)
52252.45	1.463e+00	3.895e–01	19.1	-0.824(0.158)
52283.54	8.534e–01	3.428e–01	35.1	-0.673(0.158)
52288.52	4.887e–01	4.158e–01	37.7	-0.671(0.158)
52289.49	3.326e–01	3.136e–01	38.2	-0.671(0.158)
52323.44	0.000e+00	6.813e–01	55.8	
52378.30	1.412e+00	2.932e–01	84.1	

[1]Magnitudes may be calculated from all flux values by $mag = -2.5\log(flux) + 25.0$

[2]Magnitude uncertainties may be calculated from all flux uncertainties by $\sigma(mag) = 2.5\log(1 + \sigma(flux)/flux)$.

TABLE 8
SN 2002P OBSERVATIONS

MJD	flux[1]	$\sigma(flux)$[2]	epoch (rest)	K-correction(σ)
	I			$I \rightarrow B$
52163.54	0.000e+00	6.612e–02	-80.8	
52174.56	-2.880e–01	1.015e–01	-74.4	
52191.43	-2.691e–01	1.074e–01	-64.6	
52198.43	-1.951e–01	2.023e–01	-60.5	
52204.48	2.285e–01	2.704e–01	-57.0	
52225.31	1.538e–01	1.925e–01	-44.9	
52231.23	2.003e–01	3.201e–01	-41.5	
52232.25	-2.645e–01	2.376e–01	-40.9	
52236.23	1.447e–01	5.361e–01	-38.6	
52252.22	2.003e–01	2.586e–01	-29.2	
52263.23	2.416e–01	5.433e–01	-22.8	
52283.27	2.670e+00	1.728e–01	-11.2	-1.104(0.062)
52289.35	4.817e+00	3.686e–01	-7.6	-1.103(0.062)
52323.22	4.278e+00	4.602e–01	12.1	-1.208(0.062)
	R			
52204.49	1.175e–01	1.522e–01	-57.0	
52231.26	3.127e–01	1.133e–01	-41.4	
52232.21	4.563e–01	8.434e–02	-40.9	
52236.20	4.347e–01	2.573e–01	-38.6	
52252.20	2.276e–01	2.515e–01	-29.3	
52283.33	2.880e+00	1.755e–01	-11.2	
52288.38	4.797e+00	1.679e–01	-8.2	
52289.28	5.011e+00	1.657e–01	-7.7	
	Z			$Z \rightarrow V$
52198.50	-2.050e–01	1.618e+00	-60.5	
52204.42	1.139e–02	3.297e–01	-57.1	
52231.29	7.322e–02	4.482e–01	-41.4	
52232.28	2.685e–02	4.122e–01	-40.8	
52236.25	6.297e–01	5.668e–01	-38.5	
52252.25	-3.498e–02	2.525e–01	-29.2	
52283.29	2.943e+00	3.967e–01	-11.2	-1.090(0.063)
52288.30	5.174e+00	2.937e–01	-8.3	-1.090(0.063)
52289.31	4.721e+00	5.307e–01	-7.7	-1.089(0.063)

[1]Magnitudes may be calculated from all flux values by $mag = -2.5\log(flux) + 25.0$

[2]Magnitude uncertainties may be calculated from all flux uncertainties by $\sigma(mag) = 2.5\log(1 + \sigma(flux)/flux)$.

TABLE 8
SN 2002W OBSERVATIONS

MJD	flux[1]	$\sigma(flux)^2$	epoch (rest)	K-correction(σ)
	I			$I \rightarrow B$
52191.56	-8.985e–02	6.036e–01	-53.7	
52198.62	8.539e–02	5.771e–01	-50.2	
52204.63	2.058e–01	1.752e–01	-47.2	
52225.56	-1.201e+00	3.222e–01	-36.9	
52231.61	2.252e–01	9.028e–02	-33.9	
52232.54	1.137e–01	2.142e–01	-33.5	
52236.51	1.473e–01	1.239e–01	-31.5	
52252.54	3.013e–01	1.912e–01	-23.6	
52263.51	-2.350e–01	9.028e–01	-18.2	
52283.50	2.721e+00	4.797e–01	-8.4	-1.152(0.122)
52288.48	3.312e+00	2.691e–01	-5.9	-1.183(0.122)
52289.42	3.884e+00	3.204e–01	-5.5	-1.183(0.122)
52323.56	2.733e+00	8.196e–01	11.3	-1.071(0.122)
52369.31	1.990e–02	2.673e–01	33.9	-0.960(0.122)
	R			
52231.60	1.270e–01	2.522e–01	-33.9	
52236.57	3.257e–02	1.742e–01	-31.5	
52252.58	-6.641e–02	4.259e–01	-23.6	
52283.60	1.773e+00	3.027e–01	-8.3	
52288.41	2.056e+00	2.692e–01	-6.0	
52289.60	2.060e+00	2.983e–01	-5.4	
52323.54	1.618e+00	1.315e+00	11.3	
52378.25	-2.108e–01	5.459e–01	38.3	
	Z			$Z \rightarrow V$
52231.57	-1.491e–02	1.477e–01	-34.0	
52236.53	3.246e–02	1.099e+00	-31.5	
52252.50	-1.937e+00	2.024e+00	-23.6	
52283.47	2.982e+00	1.853e–01	-8.4	-1.231(0.209)
52288.44	4.191e+00	8.122e–01	-6.0	-1.282(0.209)
52289.61	5.073e+00	1.148e+00	-5.4	-1.284(0.209)
52323.50	3.850e+00	1.067e+00	11.3	-1.180(0.209)
52369.34	-2.245e+00	2.416e+00	33.9	
52377.31	6.050e–01	9.599e–01	37.8	-0.546(0.209)

[1]Magnitudes may be calculated from all flux values by $mag = -2.5\log(flux) + 25.0$

[2]Magnitude uncertainties may be calculated from all flux uncertainties by $\sigma(mag) = 2.5\log(1 + \sigma(flux)/flux)$.

TABLE 8
SN 2002X OBSERVATIONS

MJD	flux[1]	$\sigma(flux)$[2]	epoch (rest)	K-correction(σ)
	I			$I \rightarrow B$
52191.56	-5.275e–04	3.540e–02	-30.1	
52198.62	1.446e–01	2.407e–01	-26.3	
52204.63	-1.292e–02	1.469e–01	-23.1	
52225.56	5.081e–02	3.983e–01	-11.8	-1.223(0.027)
52231.61	2.602e–02	1.929e–01	-8.6	-1.235(0.027)
52232.54	1.588e–01	2.460e–01	-8.1	-1.237(0.027)
52236.51	1.623e–01	2.018e–01	-5.9	-1.243(0.027)
52252.54	1.110e–01	1.859e–01	2.7	-1.257(0.027)
52263.51	3.747e–01	7.063e–01	8.6	-1.246(0.027)
52283.50	2.640e+00	1.823e–01	19.3	-1.182(0.027)
52288.48	3.398e+00	9.382e–02	22.0	-1.182(0.027)
52289.42	3.752e+00	1.451e–01	22.5	-1.183(0.027)
52323.56	1.359e+00	1.014e+00	40.9	
52369.31	4.473e–01	1.912e–01	65.5	
	R			
52231.60	1.785e–03	3.986e–02	-8.6	
52236.57	1.147e–01	7.822e–02	-5.9	
52252.58	-1.647e–02	1.211e–01	2.7	
52283.60	1.568e+00	3.986e–02	19.4	
52288.41	1.951e+00	1.340e–01	22.0	
52289.60	1.987e+00	9.815e–02	22.6	
52323.54	4.364e–01	1.641e–01	40.9	
52378.25	8.871e–02	1.069e–01	70.3	
	Z			$Z \rightarrow V$
52231.57	0.000e+00	1.811e–02	-8.6	-1.092(0.164)
52236.53	-6.353e–01	2.661e–01	-5.9	-1.158(0.164)
52252.50	-7.105e–01	6.353e–01	2.7	-1.038(0.164)
52283.47	2.732e+00	2.647e–01	19.3	-0.799(0.164)
52288.44	3.860e+00	1.588e–01	22.0	-0.785(0.164)
52289.61	4.298e+00	2.020e–01	22.6	-0.785(0.164)
52323.50	2.384e+00	3.901e–01	40.8	
52369.34	9.641e–01	3.385e–01	65.5	
52377.31	-2.480e–01	2.494e–01	69.8	

[1]Magnitudes may be calculated from all flux values by $mag = -2.5\log(flux) + 25.0$

[2]Magnitude uncertainties may be calculated from all flux uncertainties by $\sigma(mag) = 2.5\log(1 + \sigma(flux)/flux)$.

TABLE 8
SN 2002AA OBSERVATIONS

MJD	flux[1]	$\sigma(flux)$[2]	epoch (rest)	K-correction(σ)
	I			$I \rightarrow B$
52195.57	3.366e–01	3.694e–01	-40.0	
52225.48	-2.170e+00	4.113e–01	-24.6	
52231.48	-3.183e–02	9.303e–02	-21.6	
52232.46	-1.020e–01	1.952e–01	-21.1	
52236.49	-1.775e+00	5.116e–01	-19.1	
52252.43	5.336e–01	4.478e–01	-10.8	-1.241(0.069)
52262.50	3.659e+00	2.061e–01	-5.7	-1.243(0.069)
52283.53	3.326e+00	1.404e–01	5.2	-1.198(0.069)
52288.51	3.306e+00	1.158e–01	7.7	-1.186(0.069)
52289.56	2.883e+00	2.663e–01	8.3	-1.181(0.069)
52323.41	5.938e–01	3.694e–01	25.6	-1.067(0.069)
52369.27	-3.638e–01	2.891e–01	49.2	
	R			
52231.46	2.482e–01	1.344e–01	-21.6	
52232.44	-6.135e–02	1.090e–01	-21.1	
52236.42	2.637e–01	2.735e–01	-19.1	
52252.41	6.858e–01	2.332e–01	-10.8	
52283.58	1.570e+00	9.329e–02	5.2	
52288.58	1.110e+00	9.000e–02	7.7	
52289.58	1.063e+00	4.665e–02	8.3	
52323.38	-3.603e–17	1.995e–01	25.6	
52377.27	2.553e–01	5.729e–02	53.3	
	Z			$Z \rightarrow V$
52231.52	-2.083e–02	5.004e–01	-21.6	
52232.50	3.168e–02	6.171e–01	-21.1	
52236.45	3.978e–01	4.683e–01	-19.0	
52252.46	-2.980e–01	5.281e–01	-10.8	
52283.56	4.739e+00	6.098e–01	5.2	-1.269(0.166)
52288.54	4.725e+00	1.886e+00	7.7	-1.251(0.166)
52289.50	4.154e+00	1.888e+00	8.2	-1.242(0.166)
52323.46	4.285e–01	5.004e–01	25.7	-0.757(0.166)
52378.31	4.518e–01	5.004e–01	53.9	

[1]Magnitudes may be calculated from all flux values by $mag = -2.5\log(flux) + 25.0$

[2]Magnitude uncertainties may be calculated from all flux uncertainties by $\sigma(mag) = 2.5\log(1 + \sigma(flux)/flux)$.

TABLE 8
SN 2002AB OBSERVATIONS

MJD	flux[1]	$\sigma(flux)$[2]	epoch (rest)	K-correction(σ)
	I			$I \rightarrow V$
52195.57	-3.882e–02	1.943e–01	-63.9	
52225.48	1.281e–01	4.897e–01	-42.9	
52231.48	-1.752e+00	2.298e–01	-38.7	
52232.46	2.813e–01	2.718e–01	-38.0	
52236.49	1.892e–01	2.563e–01	-35.1	
52252.43	7.209e–01	1.733e–01	-23.9	
52262.50	2.593e–02	2.289e–01	-16.9	-0.789(0.048)
52283.53	1.837e+01	9.211e–02	-2.1	-0.847(0.048)
52288.51	2.049e+01	6.840e–02	1.4	-0.840(0.048)
52289.56	1.871e+01	2.800e–01	2.2	-0.835(0.048)
52323.41	7.311e+00	1.842e–01	26.0	-0.872(0.048)
52369.27	2.414e+00	1.514e–01	58.2	
	R			$R \rightarrow B$
52231.46	-2.517e–01	1.044e–01	-38.7	
52232.44	9.811e–02	8.569e–02	-38.0	
52236.42	-3.552e–01	2.882e–01	-35.1	
52252.41	-3.603e–17	3.293e–01	-23.9	
52283.58	1.596e+01	7.403e–02	-2.0	-0.681(0.037)
52288.58	1.648e+01	4.310e–02	1.5	-0.687(0.037)
52289.58	1.617e+01	5.248e–02	2.2	-0.687(0.037)
52323.38	2.852e+00	2.031e–01	25.9	-0.799(0.037)
52377.27	7.428e–01	8.619e–02	63.8	
	Z			
52231.52	-4.114e–01	3.209e–01	-38.7	
52232.50	-5.183e–17	3.924e–01	-37.9	
52236.45	1.040e+00	3.209e–01	-35.2	
52252.46	-6.565e–01	4.858e–01	-23.9	
52283.56	1.871e+01	4.143e–01	-2.1	
52288.54	1.907e+01	1.357e–01	1.4	
52289.50	1.932e+01	2.378e–01	2.1	
52323.46	7.630e+00	4.420e–01	26.0	
52378.31	1.501e+00	2.349e–01	64.5	

[1]Magnitudes may be calculated from all flux values by $mag = -2.5\log(flux) + 25.0$

[2]Magnitude uncertainties may be calculated from all flux uncertainties by $\sigma(mag) = 2.5\log(1 + \sigma(flux)/flux)$.

TABLE 8
SN 2002AD OBSERVATIONS

MJD	flux[1]	$\sigma(flux)$[2]	epoch (rest)	K-correction(σ)
	I			$I \rightarrow V$
52232.55	3.209e–01	3.876e–01	-24.1	
52236.63	-1.001e+00	6.846e–01	-21.4	
52252.61	4.556e+00	2.909e–01	-10.9	-0.863(0.037)
52263.57	1.123e+01	3.057e–01	-3.6	-0.867(0.037)
52283.63	9.458e+00	3.449e–01	9.6	-0.880(0.037)
52288.62	8.537e+00	2.865e–01	12.9	-0.882(0.037)
52323.56	1.694e+00	4.599e–01	36.0	-0.826(0.037)
52377.39	2.523e+00	3.527e–01	71.5	
	R			$R \rightarrow B$
52252.59	3.489e+00	7.515e–02	-10.9	-0.706(0.020)
52283.61	6.134e+00	5.705e–01	9.6	-0.674(0.020)
52288.59	4.382e+00	2.078e–01	12.9	-0.680(0.020)
52289.63	3.874e+00	1.894e–01	13.6	-0.681(0.020)
52323.59	-2.477e–01	6.626e–01	36.0	
52378.27	4.886e–02	2.942e–01	72.1	
	Z			
52232.58	9.476e–02	3.344e–01	-24.1	
52252.64	5.241e+00	2.393e–01	-10.8	
52288.65	7.579e+00	4.533e–01	12.9	
52323.62	7.572e–01	9.937e–01	36.0	
52369.36	9.411e–01	1.319e+00	66.0	
52377.33	1.342e+00	2.995e–01	71.5	
52378.34	-1.417e+00	1.293e+00	72.5	

[1]Magnitudes may be calculated from all flux values by $m = -2.5\log(flux) + 25.0$

[2]Magnitude uncertainties may be calculated from all flux uncertainties by $\sigma(mag) = 2.5\log(1 + \sigma(flux)/flux)$.

TABLE 9
HST WFPC2 F850LP OBSERVATIONS

SN	MJD	Integration (sec)	mag	$\sigma(mag)$	epoch (rest)	K-correction(σ)
2001hu	52280.23	5600.0	23.880	0.106	15.8	-0.929(0.138)
	52287.10	5600.0	24.304	0.152	19.4	-0.851(0.138)
	52294.45	5600.0	24.422	0.163	23.3	-0.773(0.138)
	52301.45	7500.0	24.663	0.173	27.0	-0.710(0.138)
	52305.19	7500.0	24.499	0.148	29.0	-0.682(0.138)
2001jf	52271.07	5600.0	23.551	0.105	2.5	-0.864(0.104)
	52277.08	5600.0	23.615	0.126	5.9	-0.905(0.104)
	52284.09	5600.0	24.121	0.168	9.7	-0.902(0.104)
	52291.50	5600.0	24.198	0.173	13.8	-0.856(0.104)
	52299.32	7500.0	24.276	0.148	18.1	-0.794(0.104)
	52303.26	7500.0	24.301	0.157	20.3	-0.763(0.104)
2001jh	52246.70	5600.0	23.894	0.134	4.4	-0.975(0.136)
	52253.52	5600.0	24.091	0.148	8.0	-0.968(0.136)
	52259.79	5600.0	23.376	0.195	11.3	-0.885(0.136)
	52266.48	5600.0	24.424	0.184	14.9	-0.776(0.136)
	52275.69	7500.0	25.582	0.323	19.8	-0.671(0.136)
	52282.63	7500.0	25.644	0.428	23.5	-0.629(0.136)

TABLE 10
SN Ia MLCS Fit Parameters

SN	redshift	t_{max}	m-M(σ)[1]	$A_V(\sigma)$	Δ	χ^2/N
2001fo[3]	0.772	52210.5	42.81(0.22)	0.04(0.26)	-0.08	0.82
2001fs[4]	0.874	52206.6	43.18(0.36)	0.08(0.42)	0.59	3.91
2001hs[3]	0.833	52243.5	43.18(0.30)	0.01(0.25)	0.15	0.58
2001hu[2]	0.882	52238.5	43.46(0.38)	0.00(0.36)	0.30	1.17
2001hx[3]	0.799	52233.5	43.65(0.36)	0.03(0.29)	0.01	1.49
2001hy[3]	0.812	52234.5	43.52(0.41)	0.01(0.35)	0.31	1.11
2001iv[2]	0.3965	52251.6	41.45(0.17)	0.03(0.17)	-0.03	2.49
2001iw[2]	0.3396	52250.5	41.24(0.17)	0.18(0.16)	-0.28	3.94
2001ix[4]	0.711	52268.6	43.22(0.25)	0.11(0.30)	-0.59	2.70
2001iy[2]	0.568	52251.6	42.21(0.23)	0.00(0.24)	-0.04	2.04
2001jb[3]	0.698	52252.5	43.24(0.45)	0.00(0.42)	-0.04	1.52
2001jf[3]	0.815	52266.5	43.80(0.30)	0.02(0.40)	-0.33	1.42
2001jh[2]	0.885	52250.5	43.59(0.23)	0.02(0.20)	-0.47	1.06
2001jm[4]	0.978	52258.4	43.49(0.31)	0.01(0.28)	-0.12	0.90
2001jn[3]	0.645	52264.4	42.83(0.32)	0.00(0.41)	0.36	1.71
2001jp[2]	0.528	52272.6	42.53(0.21)	0.00(0.32)	-0.56	2.59
2001kd[3]	0.936	52215.5	43.79(0.44)	0.01(0.41)	-0.21	0.43
2002P[2]	0.719	52302.5	43.06(0.49)	0.02(0.47)	-0.35	2.41
2002W[3]	1.031	52300.5	43.96(0.89)	0.01(0.50)	-0.58	0.37
2002X[3]	0.859	52299.5	42.76(0.64)	0.01(0.33)	0.60	1.44
2002aa[3]	0.946	52273.5	43.89(0.55)	0.01(0.62)	-0.38	1.35
2002ab[2]	0.423	52286.5	41.87(0.19)	0.08(0.16)	-0.44	1.07
2002ad[2]	0.514	52269.1	42.16(0.25)	0.01(0.41)	-0.08	1.15

[1]all distances calculated using $H_0 = 72$ km s^{-1} Mpc^{-1} (Freedman et al. 2001)

[2]9 SNe for which there is unambiguous spectral confirmation as a SN Ia at the host-galaxy redshift.

[3]11 SNe for which there is substantial photometric evidence, but not unambiguous spectral confirmation, for identification as a SN Ia at the host galaxy redshift.

[4]3 SNe for which there is clear spectral identification as a SN Ia, but no host galaxy emission with which to confirm the redshift.

TABLE 11
SN IA LIGHT CURVE FIT PARAMETERS

SN	redshift	m-M$_{BATM}(\sigma)$[1]	$A_{V,BATM}(\sigma)$	m-M$_{dm15}(\sigma)$[1]	$E(B-V)_{dm15}(\sigma)$	dm15
2001fo[3]	0.772	43.00(0.20)	0.04(0.08)	42.88(0.18)	0.07(0.03)	1.08(0.12)
2001fs[4]	0.874	43.84(0.50)	0.49(0.34)	...	...	...
2001hs[3]	0.833	43.45(0.34)	0.20(0.27)	...	...	...
2001hu[2]	0.882	43.74(0.51)	0.40(0.34)	...	...	...
2001hx[3]	0.799	43.81(0.44)	0.29(0.31)	43.24(0.33)	0.20(0.07)	1.27(0.32)
2001hy[3]	0.812	43.96(0.37)	0.18(0.26)	...	...	...
2001iv[2]	0.3965	41.20(0.22)	0.54(0.21)	41.31(0.25)	0.20(0.05)	1.09(0.16)
2001iw[2]	0.3396	40.78(0.32)	0.58(0.22)	40.88(0.21)	0.23(0.03)	1.13(0.20)
2001ix[4]	0.711	43.14(0.28)	0.14(0.21)	43.09(0.20)	0.00(0.04)	0.99(0.17)
2001iy[2]	0.568	42.35(0.17)	0.09(0.14)	42.23(0.21)	0.00(0.03)	1.19(0.14)
2001jb[3]	0.698	43.09(0.42)	0.30(0.31)	42.84(0.25)	0.22(0.05)	1.19(0.18)
2001jf[3]	0.815	43.90(0.32)	0.15(0.22)	...	...	...
2001jh[2]	0.885	43.40(0.45)	0.20(0.26)	...	...	...
2001jm[4]	0.978	43.87(0.26)	0.09(0.17)	...	...	...
2001jn[3]	0.645	43.00(0.35)	0.48(0.30)	42.68(0.20)	0.36(0.04)	0.89(0.11)
2001jp[2]	0.528	42.42(0.15)	0.03(0.07)	42.40(0.15)	0.02(0.03)	0.85(0.10)
2001kd[3]	0.936	43.73(0.42)	0.27(0.30)	...	...	...
2002P[2]	0.719	42.99(0.33)	0.13(0.20)	42.97(0.23)	0.00(0.03)	1.10(0.16)
2002W[3]	1.031	43.66(0.48)	0.19(0.27)	...	...	...
2002X[3]	0.859	43.63(0.43)	0.28(0.31)	...	...	...
2002aa[3]	0.946	43.86(0.20)	0.06(0.13)	...	...	...
2002ab[2]	0.423	41.55(0.15)	0.07(0.12)	41.78(0.19)	0.05(0.04)	0.99(0.14)
2002ad[2]	0.514	42.29(0.35)	0.29(0.28)	42.12(0.40)	0.11(0.10)	1.10(0.28)

[1]all distances calculated using $H_0 = 72$ km s^{-1} Mpc^{-1} (Freedman et al. 2001)

[2]9 SNe for which there is unambiguous spectral confirmation as a SN Ia at the host-galaxy redshift.

[3]11 SNe for which there is substantial photometric evidence, but not unambiguous spectral confirmation, for identification as a SN Ia at the host galaxy redshift.

[4]3 SNe for which there is clear spectral identification as a SN Ia, but no host galaxy emission with which to confirm the redshift.

TABLE 12
SN IA SUMMARY

SN	l^{II}	b^{II}	z	$\log(cz)$	$\langle\log(dH_0)\rangle$	$\pm$	$\langle A_V\rangle$
2001fo[2]	197.647	-30.139	0.772	5.364	5.434	0.030	0.10
2001fs[3]	197.895	-29.739	0.874	5.418	5.560	0.076	0.28
2001hs[2]	197.949	-29.806	0.833	5.397	5.521	0.057	0.11
2001hu[1]	210.560	17.621	0.882	5.422	5.577	0.078	0.20
2001hx[2]	176.770	39.195	0.799	5.379	5.587	0.060	0.32
2001hy[2]	176.490	39.264	0.812	5.386	5.605	0.069	0.10
2001iv[1]	210.219	17.674	0.3965	5.076	5.120	0.034	0.41
2001iw[1]	210.217	17.792	0.3396	5.008	5.034	0.033	0.50
2001ix[3]	149.779	53.346	0.711	5.329	5.485	0.042	0.08
2001iy[1]	149.577	53.253	0.568	5.231	5.304	0.033	0.03
2001jb[2]	166.500	-54.195	0.698	5.321	5.476	0.064	0.34
2001jf[2]	167.004	-53.939	0.815	5.388	5.628	0.055	0.09
2001jh[1]	167.404	-53.880	0.885	5.424	5.557	0.059	0.11
2001jm[3]	197.771	-29.755	0.978	5.467	5.593	0.051	0.05
2001jn[2,4]	197.822	-29.500	0.645	5.286	5.423	0.053	0.55
2001jp[1]	176.714	38.677	0.528	5.199	5.341	0.023	0.03
2001kd[2]	210.190	17.767	0.936	5.448	5.609	0.076	0.14
2002P[1]	166.969	-53.518	0.719	5.334	5.455	0.050	0.05
2002W[2]	176.516	38.931	1.031	5.490	5.619	0.123	0.10
2002X[2]	176.481	39.039	0.859	5.411	5.496	0.096	0.14
2002aa[2]	210.043	17.353	0.946	5.453	5.633	0.068	0.04
2002ab[1]	210.250	17.306	0.423	5.103	5.214	0.030	0.10
2002ad[1]	149.609	52.870	0.514	5.188	5.289	0.053	0.22

[1]9 SNe for which there is unambiguous spectral confirmation as a SN Ia at the host-galaxy redshift.

[2]11 SNe for which there is substantial photometric evidence, but not unambiguous spectral confirmation, for identification as a SN Ia at the host galaxy redshift.

[3]3 SNe for which there is clear spectral identification as a SN Ia, but no host galaxy emission with which to confirm the redshift.

[4]SN 2001jn is not included in our cosmological fits due to $\langle A_V\rangle > 0.5$.

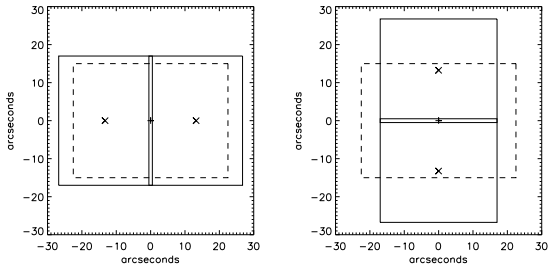

Fig. 1.— Configuration of the Suprime-Cam and CFHT+12K fields of view during the IfA Deep Survey. Solid lines depict the two Suprime-Cam fields of view, dashed lines show the coverage of the single 12K field of view. Shown on the left is the layout for Fields 0230, 0438, 0749, and 0848. Shown on the right is the layout for Field 1052.

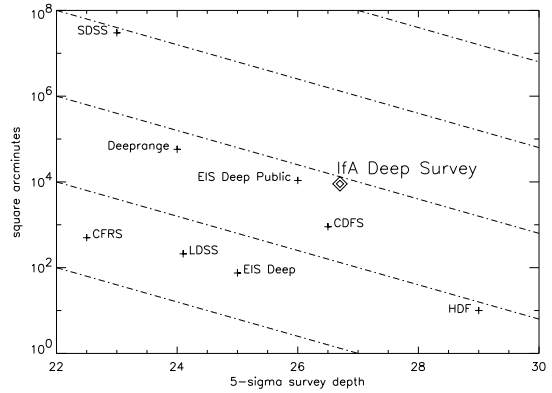

Fig. 2.— A plot of depth (approximate AB magnitudes) versus size for several recent and historical surveys. Diagonal lines show contours of constant volume. The IfA Deep Survey covers a unique region of this parameter space. SDSS (Sloan Digital Sky Survey, www.sdss.org, York et al. 2000). Deeprange (Postman et al. 1998). EIS (ESO Imaging Survey) Deep, Deep Public (www.eso.org/eis). CFRS (Canada-France Redshift Survey, Lilly et al. 1995). LDSS (Low Dispersion Survey Spectrograph, Glazebrook et al. 1995). CDFS (GOODS/ESO Chandra Deep Field South, www.eso.org/eis). HDF (Hubble Deep Field, Williams et al. 1996).

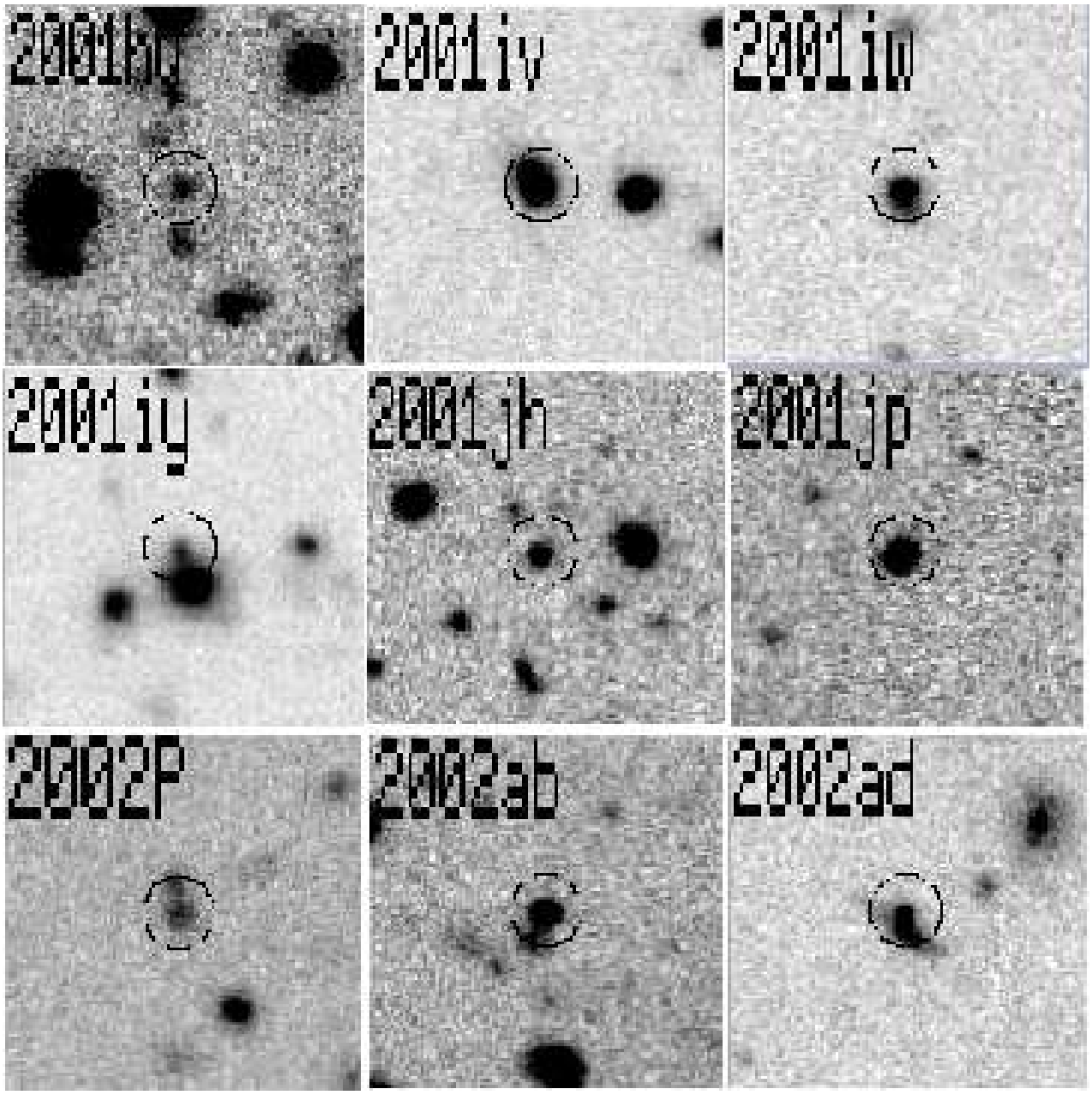

Fig. 3.— I-band Subaru images centered on the location of each of the 9 IfA Deep Survey SNID-confirmed SNe Ia (indicated with a circle), taken as close to peak brightness as possible. Images are $20''$ on a side. North is up and East to the left.

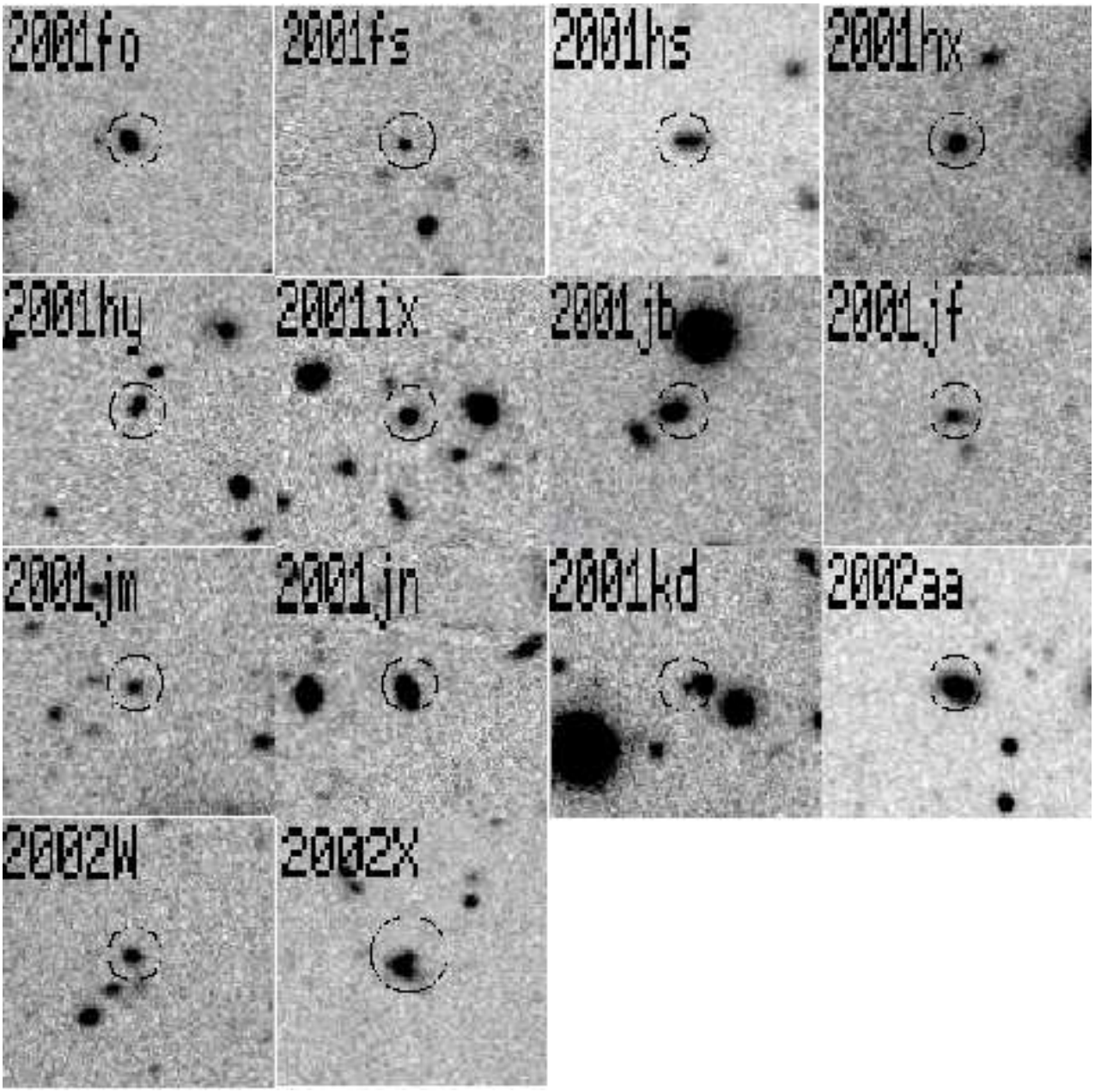

Fig. 4.— I-band Subaru images centered on the location of each of the 14 additional SNe Ia (indicated with a circle), taken as close to peak brightness as possible. Images are $20''$ on a side. North is up and East to the left.

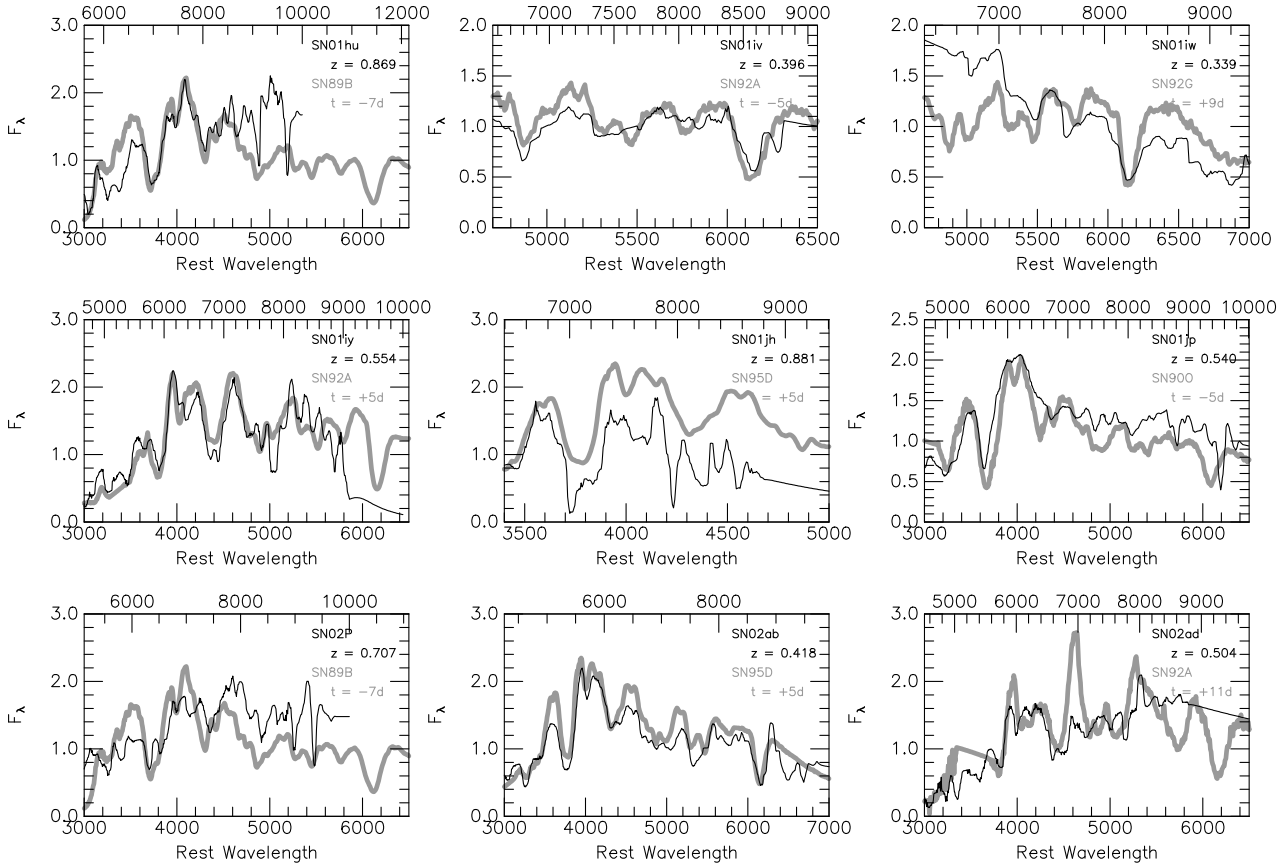

Fig. 5.— Spectra of the 9 SNe with spectral matches to local SNe Ia as determined by SNID. The spectra have been smoothed by taking a weighted median of FWHM 80 Å. Both spectra and template are shown as F_λ. Observed wavelength is indicated along top of graphs, with all wavelengths given in angstroms.

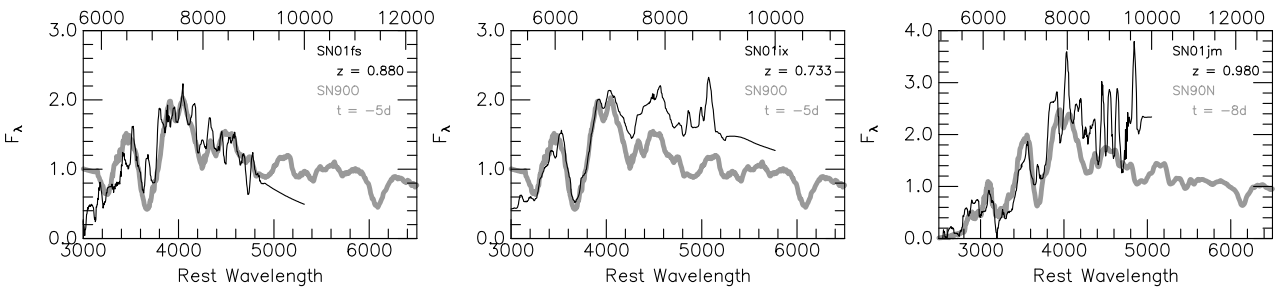

Fig. 6.— Spectra of the 3 SNe without a host-galaxy emission redshift but with spectral matches to local SNe Ia as determined by SNID. The spectra have been smoothed by taking a weighted median of FWHM 80 Å. Both spectra and template are shown as F_λ. Observed wavelength is indicated along top of graphs, with all wavelengths given in angstroms.

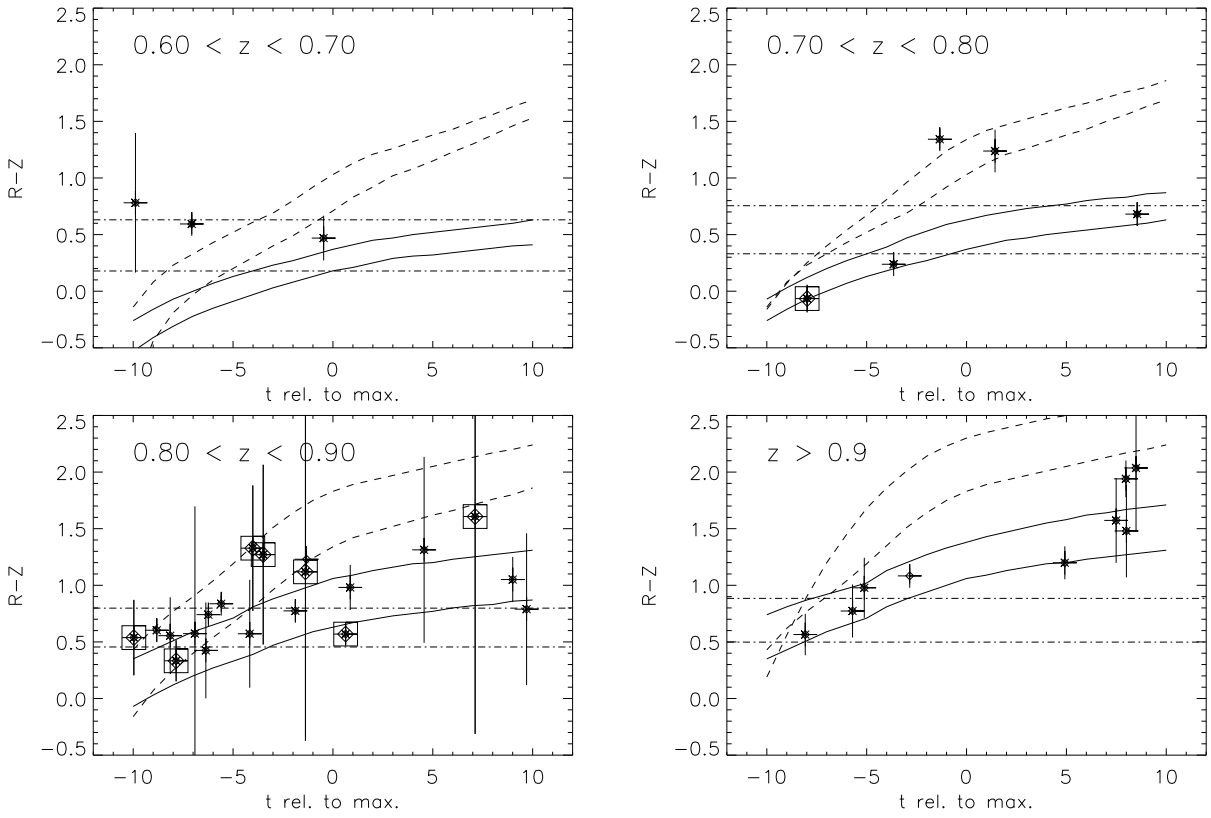

Fig. 7.— $R - Z$ colors of the IfA Deep Survey SNe Ia as a function of time relative to maximum brightness. Spectroscopically confirmed SNe Ia are indicated with a box. Several contours are shown to indicate the range of different types of SNe over the redshift range indicated in each plot. SN 1995D is a bright SN Ia (solid lines), SN 1999by is an extremely subluminous SN Ia (dashed lines). Type II SN (dashed-dotted lines) are represented by extrapolation from single measurements of SNe 1998S and 1999em, inflating the width by 0.3 magnitudes to allow for evolution. The objects without spectroscopic confirmation as SNe Ia are all photometrically consistent with being so. Except at very high redshift, they are not inconsistent with the SN II regions, however.

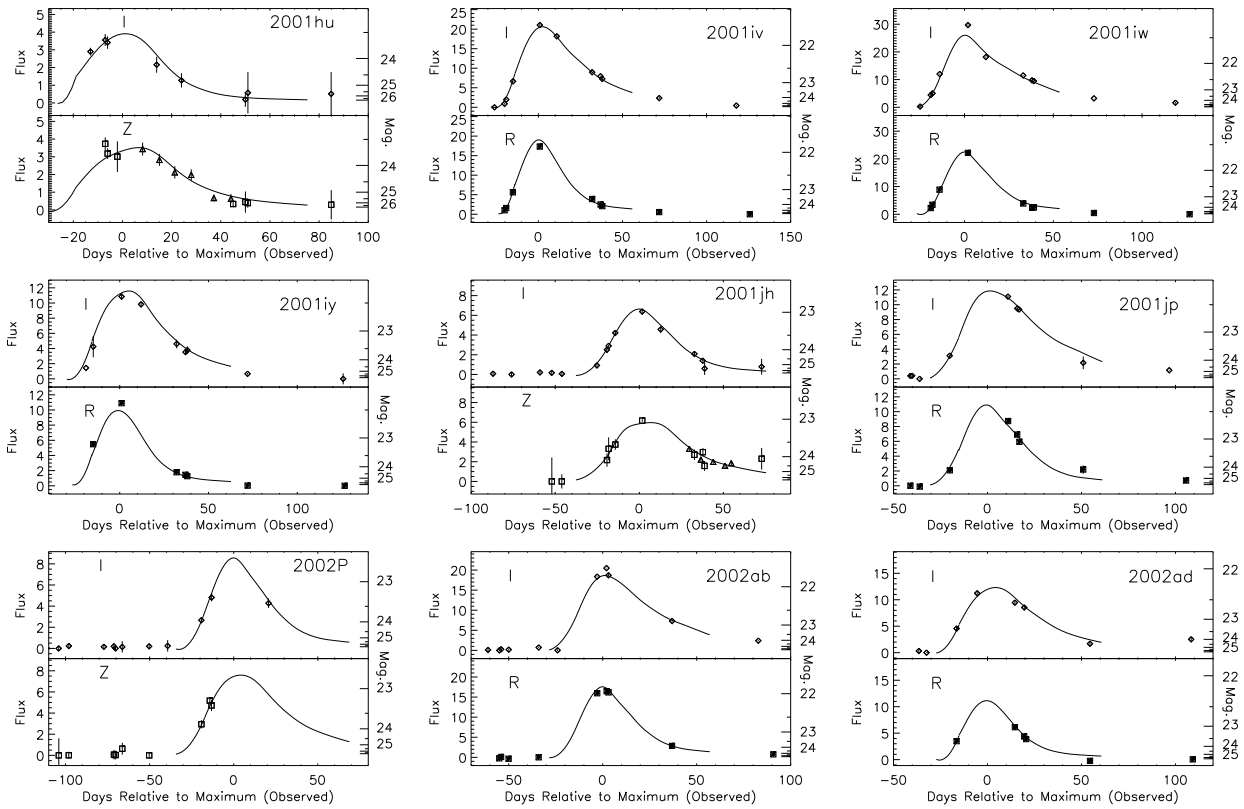

Fig. 8.— Light curves for the 9 IfA Deep Survey SNID-confirmed SNe Ia. Ground based data are plotted as observed for the two filters fit with MLCS (R,I for $z < 0.7$ and I,Z for $z > 0.7$), with the MLCS fit shown by solid lines. In addition, $F850LP$ (triangles) points for SN 2001hu and 2001jh are shown with a shift equal to the difference in K-corrections from $Z \rightarrow V$ and $F850LP \rightarrow V$ to better illustrate the fit to the data.

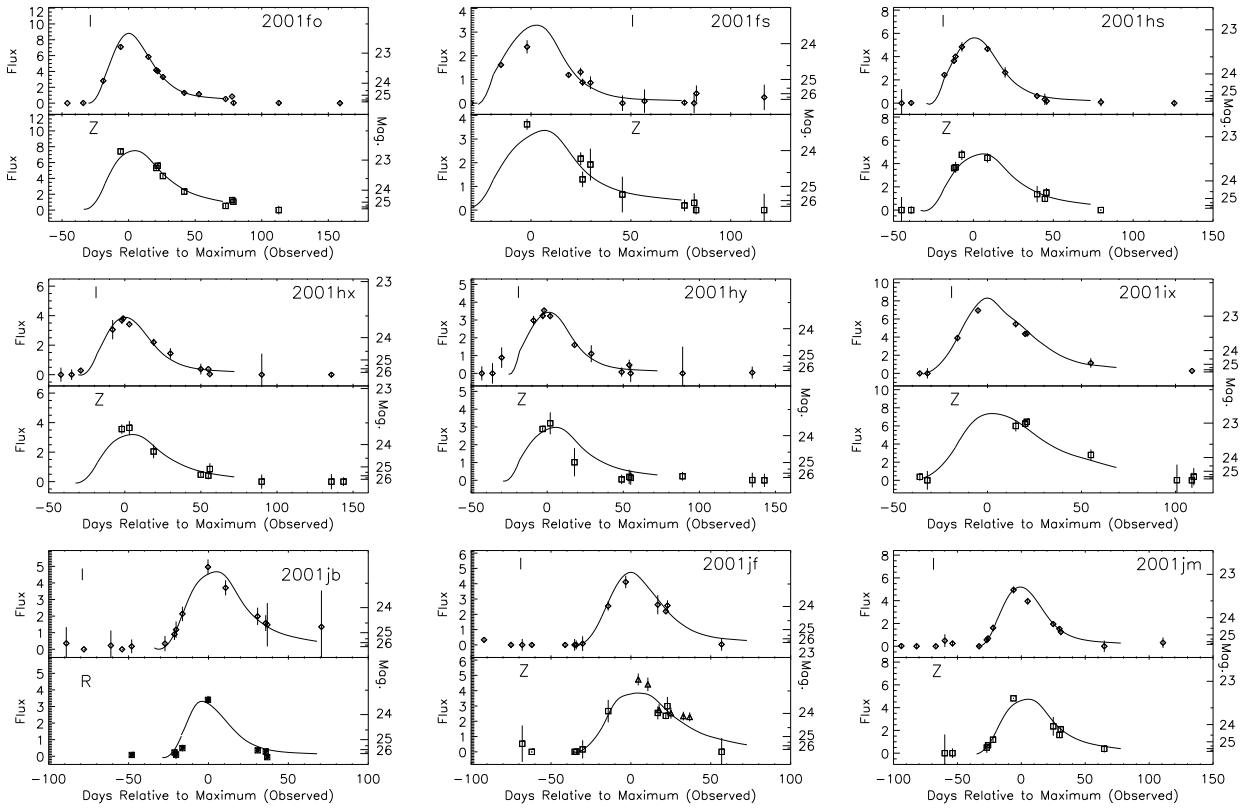
2001fo
2001fs
2001hs
2001hx
2001hy
2001ix
2001jb
2001jf
2001jm
I
Z
R
Flux
Mag.
Days Relative to Maximum (Observed)

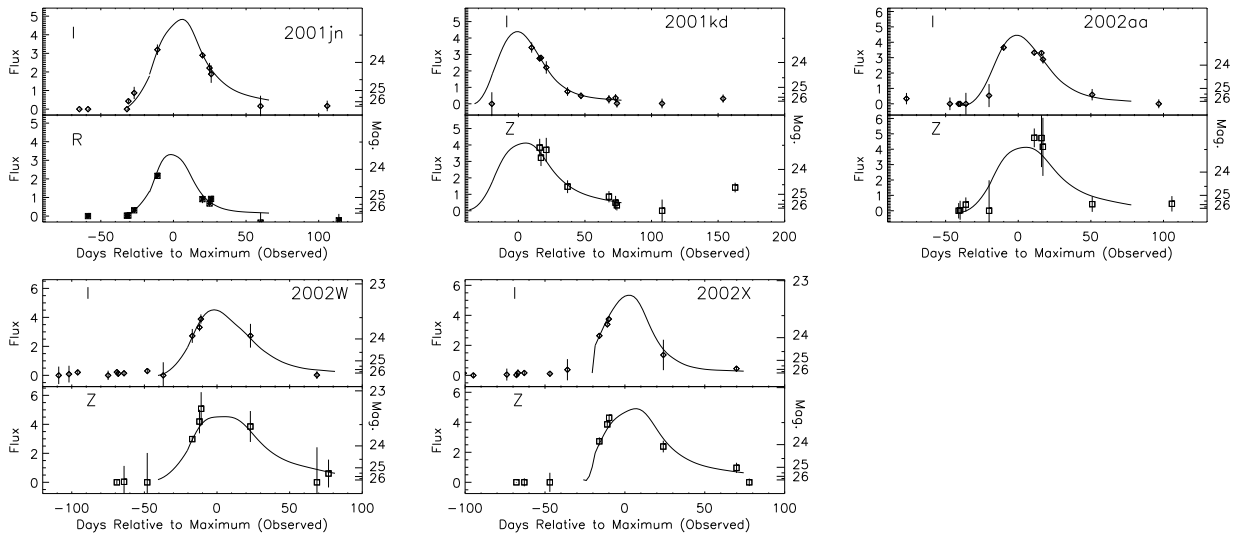

Fig. 9.— Light curves for the 14 additional SNe Ia. Ground-based data are plotted as observed for the two filters fit with MLCS (R,I for $z < 0.7$ and I,Z for $z > 0.7$), with the MLCS fit shown by solid lines. In addition, $F850LP$ (triangles) points for SN 2001jf are shown with a shift equal to the difference in K-corrections from $Z \rightarrow V$ and $F850LP \rightarrow V$ to better illustrate the fit to the data.

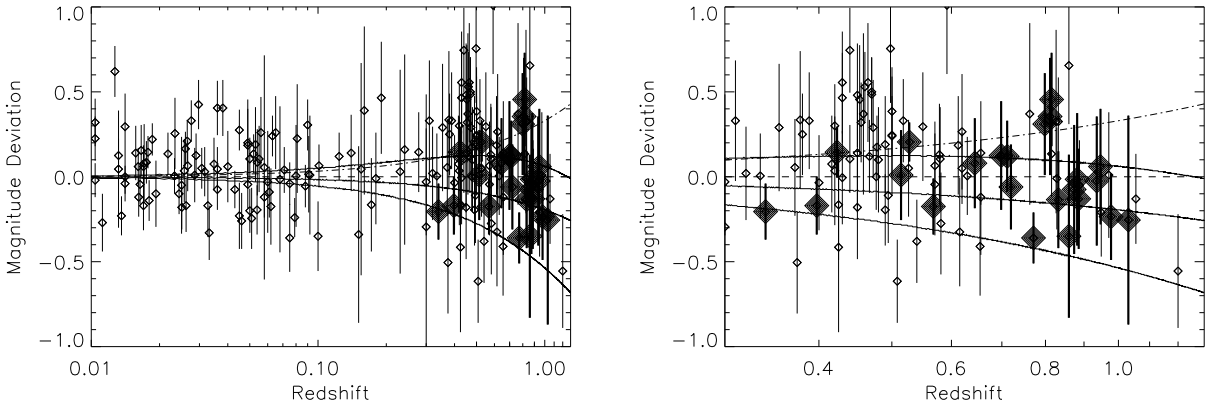

Fig. 10.— Hubble Diagram showing the magnitude deviation with respect to an empty universe of the 23 IfA Deep Survey SNe Ia (large diamonds), as well as previously published SN Ia at similar redshift collected by Tonry et al. (2003). This diagram is constructed from the values given in Table 12, and requires no assumption about the value of H_0. From top to bottom, solid lines represent cosmologies with (Ω_M,Ω_Λ)=(0.3, 0.7), (0.3, 0.0), and (1.0, 0.0), respectively. Note the maximum positive deviation of a Ω_Λ-dominated universe occurs at $z \approx 0.5$. Right-hand panel is focussed on high redshift to more clearly show the IfA Deep Survey SNe. Also shown is a dashed-dotted line showing the effects of a systematic effect proportional to z.

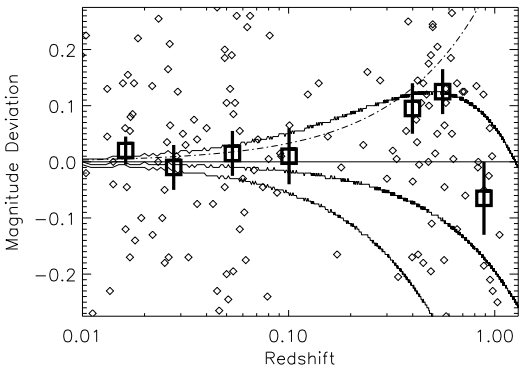

Fig. 11.— Literature supernovae (diamonds) shown along with median values binned by redshift (squares). Individual points are shown without error bars for the sake of clarity. Redshift bins contain a minimum of 20 SNe Ia. From top to bottom, solid lines represent cosmologies with $(\Omega_M,\Omega_\Lambda)$=(0.3, 0.7), (0.3, 0.0), and (1.0, 0.0), respectively. Also shown is a dashed-dotted line representing a systematic effect proportional to z, which does not correspond well with the highest redshift bins.

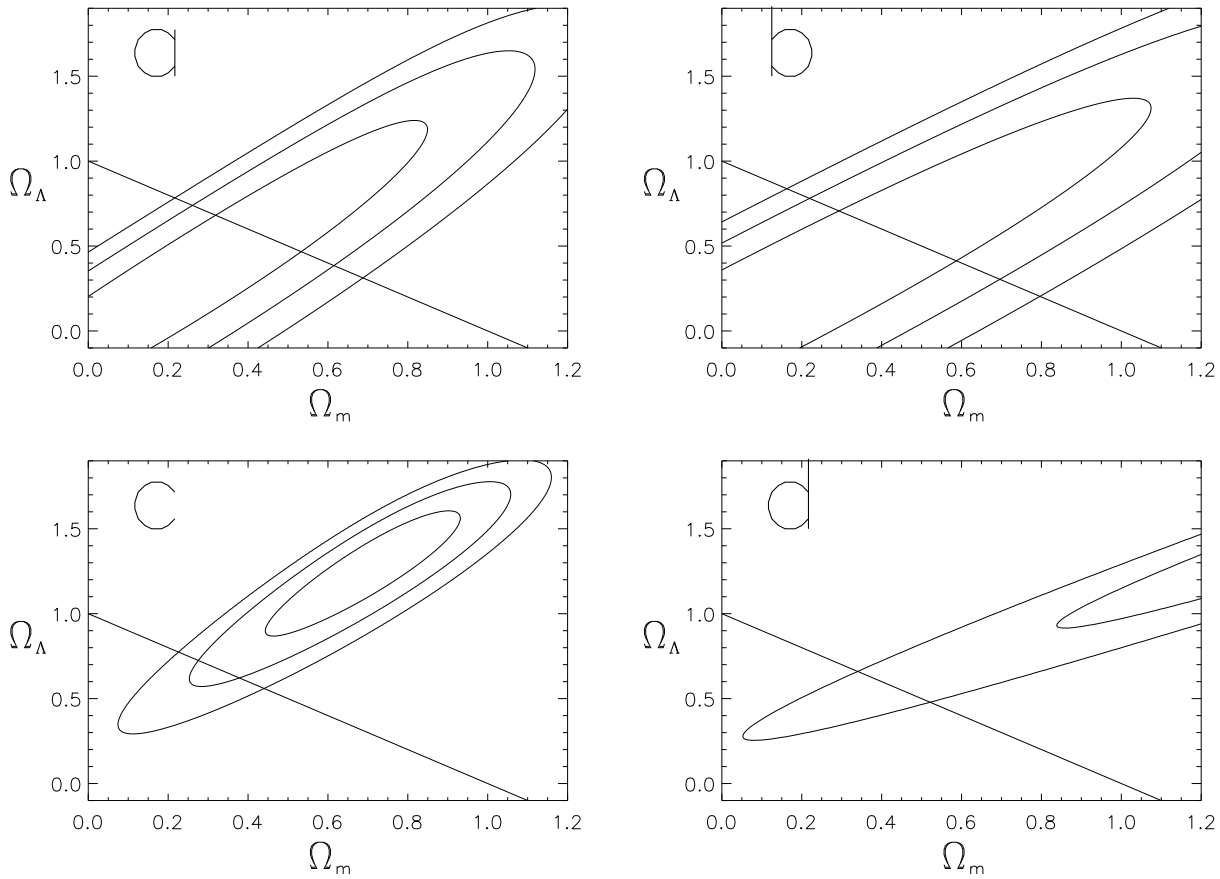

Fig. 12.— 68%, 95%, and 99.5% confidence contours for the sample of: a) 98 SNe Ia $0.01 \leq z \leq 0.3$ SNe Ia plus 22 from this survey (120 total); b) 98 SNe Ia $0.01 \leq z \leq 0.3$ SNe Ia plus 9 from this survey with SNID confirmation (107 total); c) 172 SNe Ia with $z \geq 0.01$ SNe and $A_V \leq 0.50$ from Tonry et al. 2003 plus 22 from the IfA Deep survey (194 total); d) same sample as c., calculated with the Dyer-Roeder empty-beam cosmology. These contours are shifted to lower values of Ω_Λ and higher values of Ω_M, with the trend becoming more pronounced at higher values of Ω_M, thus greatly elongating the contours.